Vortex-Plate Interaction in Wake-Induced Vibration: A Study of Single and Parallel Flat Plates Behind a Cylinder

Mohammad Jebelli[a], Koosha Shariloo[b], Mehran Masdari[c]

[a] Faculty of new sciences and technologies, University of Tehran, Tehran, Iran

[b] Department of Aerospace Engineering, Sharif University of Technology, Tehran, Iran

[c] School of Science and Technology, Department of Engineering, City University of London, London, UK

Abstract

This computational research investigates the oscillations caused by the wake of a circular cylinder on either a single or dual flat plates in a laminar flow scenario. The findings emphasize the crucial role of the flat plate placement, which can significantly impact their ability to serve as control devices or experience noticeable oscillations. When a plate is positioned beyond the crucial juncture, it causes significant amplitude oscillations. These oscillations decrease when the plate is moved further away from the horizontal axis. Furthermore, at specific short horizontal distances, there are noticeable oscillations with a moderate amplitude. These oscillations are caused by changes in the immediate wake structure. Oscillations in dual plates, which can oscillate independently, occur only when there is sufficient room for shear-layer contact. By adjusting the vertical distance, we may see different effects on vortex damping and plate oscillation. Increasing the gap size reduces the area where there is no oscillation. This experiment also encompasses a range of lower velocities, demonstrating that although the plate(s) reliably replicate the shedding frequency of the upstream cylinder in all configurations, this frequency can be affected and altered in tiny gaps. An analysis of single and dual plates reveals their effectiveness in designing energy harvesting devices, with two plates offering a slight advantage by utilizing separate components within a very similar area.

Keywords

Cylinder; Flat plate; Vortex shedding; Wake-Induced Vibration; Laminar flow

1 Introduction

Cylinders are a fundamental topic in fluid mechanics engineering for studying the flow dynamics around bluff bodies. Vortex formation in the wake zone is a prominent feature of the flow around a circular cylinder. This phenomenon has been intensively studied due to its relevance to various applications. These encompass the dynamic interactions between fluids and structures, specifically in the context of buildings like bridges, skyscrapers, and wind turbine blades (Jain et al., 1996; Yang et al., 2004; Arrigan et al., 2011). Additionally, research has been conducted on the phenomena of noise and thermal transmission (Zhang and Øiseth, 2021; Xu et al., 2019).

The Reynolds number, which is determined by the diameter of a cylinder and the velocity of the undisturbed flow, ($Re = \rho UD/\mu$),has a significant effect on the wake flow. It affects different flow characteristics, such as the shear layers and the pattern of vortex shedding. This effect becomes noticeable when the Reynolds number exceeds 47. Vortex-Induced Vibration (VIV) is a self-excited oscillation that can occur when a structure interacts with shedding vortices (Blevins, 1977). Wake-induced vibration (WIV) occurs when vortices are discharged from a bluff body located upstream (Zdravkovich, 1988; Bokaian and Geoola, 1984). A multitude of reviews have been carried out on these phenomena, as well as on Flow-induced motions, in the past few decades (Bearman, 1984; Griffin and Ramberg, 1982; Parkinson, 1989; Sarpkaya, 1979; Williamson and Govardhan, 2004).

The primary aim of early research on Flow-Induced Motions (FIMs) was to get a better understanding of these phenomena and develop effective strategies to mitigate their negative effects. Nevertheless, over the past ten years, there has been a growing interest in FIMs as a practical method for producing sustainable energy. The combination of a cylindrical

body and a connected or separate flat plate, known as a simple and effective passive method, has been extensively researched mostly for controlling and reducing FIMs, and sometimes, to enhance them for the purpose of energy harvesting.

Studies on the effects of a long splitter plate attached to the back of a cylinder have shown a notable decrease in vortex shedding and a large reduction in drag (Roshko, 1955; Apelt et al., 1973; Apelt and West, 1975). Using a separate plate has been found to be advantageous in controlling vortex shedding (Unal and Rockwell, 1988). The essential thresholds for influencing the flow surrounding a circular cylinder in laminar conditions have been determined at horizontal separations of 2.5 and 2.6D (Lin and Wu, 1994; Hwang et al., 2003). To achieve the best possible suppression, Dehkordi and Jafari discovered that the necessary horizontal distance and the vertical location of the plate are key factors that interact with each other. Their research revealed that parallel splitters can reduce drag force by up to 20% (Dehkordi and Jafari, 2010).

The use of a splitter plate is anticipated to deliberately delay the shear layer interaction, leading to a subsequent reduction in hydrodynamic forces and, consequently, alleviating the impact of flow-induced vibrations (FIV) on a circular cylinder (Tang et al., 2023).

Studies have been conducted to examine the effects of incorporating a splitter plate on Vortex-Induced Vibrations (VIV). These investigations have been done using experimental methods (Assi and Bearman, 2015; Stappenbelt, 2010; Assi et al., 2009) as well as numerical analyses (Sahu et al., 2019; Sun et al., 2020; Zhang et al., 2021). The size of the attached plate significantly influences the FIV behavior of the cylinder, causing self-restrained oscillations for shorter plates and uncontrolled galloping for longer plates (Wu et al., 2023). A plate that is sufficiently extensive will effectively suppress oscillations (Zeng et al., 2023). In contrast, a

pliable plate with a length in the direction of the flow that is greater than the diameter of the cylinder significantly reduces vibrations (Cui et al., 2022). Moreover, a study conducted on a cylinder combined with a separate flexible plate identified two clearly defined phases of reaction, distinguished by the horizontal distance between the objects. These phases were classified as Vortex-Induced Vibration (VIV) for shorter gaps and galloping for longer gaps (Mittal and Sharma, 2022).

Recently, there has been a trend in study towards developing methods for energy harvesting from different setups comprising a cylinder and a plate. An area of focus is the implementation of a piezoelectric plate on the back side of the cylinder, which has been thoroughly investigated. An et al. introduced a novel energy conversion device called the vortex-induced piezoelectric energy converter (VIPEC). This device utilizes the pressure difference generated by vortices to activate a plate, compress piezoelectric patches, and transform fluid dynamic energy into electrical energy. According to their research, changing the length of the plate affects how it interacts with shear layers and delays the shedding of vortices (An et al., 2018). Su and Lin developed a vortex-induced bi-directional piezoelectric energy harvester that can efficiently capture wind energy from two perpendicular directions. The device is designed in a U-shape and has the ability to modify the aspect ratio, which in turn allows for the control of wind lock-in speed (Su and Lin, 2020). Wang et al. proposed attaching a rectangular stationary plate behind a previous circular cylinder to enhance the energy extraction from its fluid-induced vibrations (FIV) (Wang et al., 2021). In 2016, Armandei and Fernandes conducted a study on the extraction of marine current energy using a device called WIV. They used a modified cylinder with a flat plate that has the ability to rotate. According to their research, the buffeting response was found to be influenced by the position of the elastic axis and the spring rate, rather than the gap between the plate and

cylinder (Armandei and Fernandes, 2016). Derakhshandeh conducted an additional study where they developed a self-excitation thin piezoelectric actuator that was affected by the vortex shedding occurring behind a stationary cylinder. Derakhshandeh (2022) found a strong correlation between the frequency of the vortex and the displacement of the tip, indicating a close relationship with the maximum power generated.

After examining the mentioned research, it is evident that flat plates have a broad range of uses that go beyond their traditional role in controlling and reducing Flow-Induced Motions (FIMs). They can potentially enhance the movement of cylinders and can also be used for directly harvesting energy. However, there is a lack of research on detachable plates, which are particularly sensitive to geometric and flow dynamics. Most existing studies focus on analyzing the flow field and regulating the Fluid-Induced Motion (FIM).

This study aims to elucidate two aspects by investigating the interactions between vortices and plates. The plates, either single or dual, are positioned in the flow behind a cylinder located upstream. Initially, the study aims to investigate the interaction between the flow created by the wake and the oscillating flat plates, as well as the resulting effects on the cylinder located upstream. This examination will enhance our understanding of fluid mechanics and the interaction between flow configurations and structural behaviors. The study primarily aims to determine certain conditions that are favorable for extracting energy from the passage of air behind an object. This particular segment, which is the main focus of the inquiry, has the potential to establish the foundation for the development of new energy-harvesting technologies that utilize fluid dynamic forces.

The article commences with an introduction to the issue at hand, succeeded by an exposition of the governing equations, numerical methodology, and method validation in Section 2.

Section 3 is bifurcated into two segments, focusing on the exposition of results and discussions pertinent to the WIV of the plates. The paper culminates with a synthesis of the principal findings and conclusions in Section 4.

Nomenclature

A*	Plunging Amplitude (A/D)
D	Circular Cylinder Diameter
L_P	Flat Plate Length
G	Non-Dimensional Horizontal spacing
m*	Mass Ratio
ζ	Damping Ratio
CL	Lift Coefficient
CL_{rms}	Root Mean Square of Lift Coefficient
CL_{mean}	Mean lift coefficient
CD_{mean}	Mean Drag Coefficient
Cp	Pressure Coefficient
Cp_b	Base Pressure Coefficient
ρ	Fluid Density
m	Body Mass
m_A	Added Mass
K	Transverse Stiffness Factor
U_{in}	Free Stream Velocity
U_r	Reduced Velocity
t	Physical Time
T	Non-Dimensional Time
St	Strouhal Number
VSA	Vibration per swept area

116

2 Problem description, governing equations, numerical methodology and validation

This section begins by presenting the problem statement, outlining the model configuration, and explaining the governing equations relevant to the fluid-solid interaction problem. The text explains the numerical method used to solve the equations and concludes with a validation of the method.

2.1 Problem description

This study examines the transverse free oscillation of a single or parallel flat plates mounted in the wake of an upstream fixed circular cylinder at a Reynolds number of 100, as shown in Figure 1. The study of the single plate involves examining different horizontal and vertical positions, including the centerline of the wake and four other vertical positions (H=0, 0.25, 0.5, 0.75, 1). This analysis covers a total of 40 cases to investigate the asymmetrical configurations. When considering the parallel plates, similar configurations are analyzed with a minimum vertical gap of H=0.25, resulting in 32 variations (eight horizontal positions are considered for each scenario).

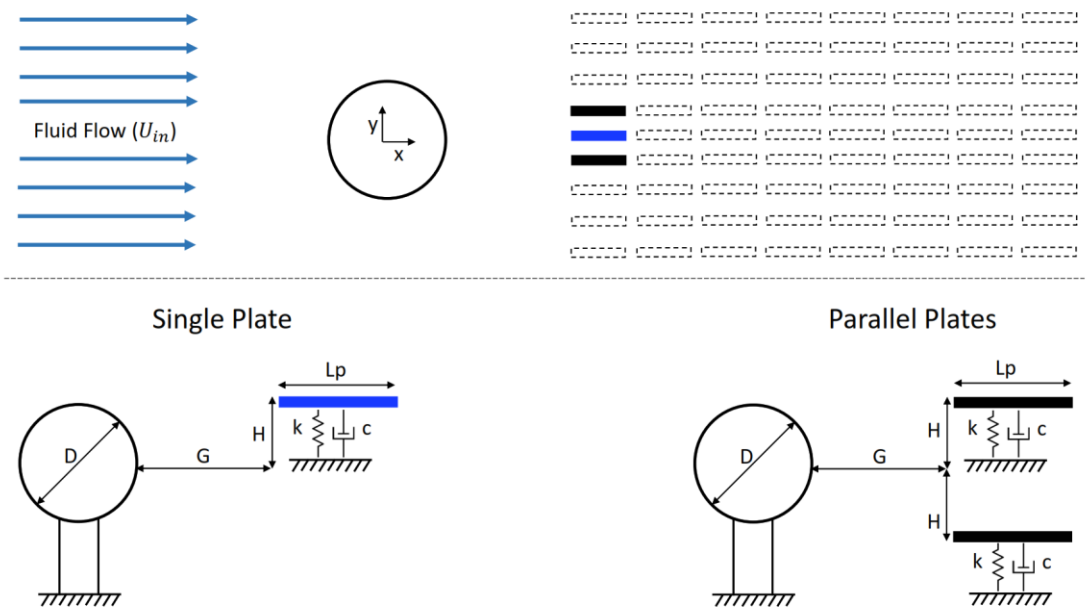

FIG. 1) Model configuration for single and parallel flat plates

The plate's length (L_P) is set equal to the cylinder's diameter (D), and the incoming flow is defined by a constant velocity represented as U_{in}. The device holding the plate(s) includes a spring with stiffness k and a mechanical damping coefficient c, which can be set to zero to allow for higher vibration amplitudes.

2.2 Governing Equations

The flow field around objects are characterised through the unsteady Navier-Stokes equations, predicated on the assumption that the flow is Newtonian and incompressible. The equations are rendered in a non-dimensional format, employing an Arbitrary Lagrangian-Eulerian (ALE) frame of reference, as articulated in equations (1) and (2).

$$\frac{\partial u_i}{\partial x_i} = 0 \tag{1}$$

$$\frac{\partial u_i}{\partial t} + \left(u_j - \hat{u}_j\right)\frac{\partial u_i}{\partial x_j} = -\frac{\partial p}{\partial x_i} + \frac{1}{Re}\frac{\partial^2 u_i}{\partial x_j^2} \tag{2}$$

The variables x, t, and p are non-dimensionalized with respect to the cylinder's diameter and the reference time ($t_{ref} = {}^{c}/_{U_\infty}$), and $\rho_\infty U_\infty^2$, respectively.

The transverse oscillation of the plate(s) is described as a system consisting of mass, spring, and damper, as shown in equation (3):

$$m\ddot{y} + c\dot{y} + ky = F_y(t) \tag{3}$$

Where y, $\dot{y}$ and $\ddot{y}$ represent the displacement, velocity, and acceleration of the plate(s) in the transverse direction, respectively. The parameter m represents the total mass that oscillates per unit length, whereas c and k represent the structural damping coefficient and the stiffness of the spring, respectively. $F_y(t)$ represents fluctuating transverse force per unit length acting on the oscillating system.

The flow field is determined at each time step by solving the flow governing equations, and the hydrodynamic forces on the plate are calculated accordingly. The computed forces are then passed to a user-defined function, and the equation of motion is solved to determine a new position for the plate. The new plate characteristics are passed back to the solver, the current location is adjusted, and the grids in the dynamic mesh zone are regenerated to prepare for calculating the flow field in the next step.

Flow-induced forces on objects are calculated by integrating the normal pressure and shear stress over their surfaces. The instantaneous lift and drag coefficients are defined as $C_L(t) = 2F_y(t)/(\rho U^2 D)$ and $C_D(t) = 2F_x(t)/(\rho U^2 D)$, respectively. Here F_y and F_x denote the force components in the cross-flow and inline directions, respectively. The plates' dynamic behavior is defined by two parameters: vibration amplitude and frequency. The vibration amplitude is made dimensionless by dividing it by the cylinder diameter, which is identical to the length of

the plate, and is defined as $A^* = A/D$. The vibration frequency variation is represented by the frequency ratio, which is normalized by the object's natural frequency (F_{os}/F_n).

The main goal of the current study is to finding configurations that have a higher capacity for energy harvesting. The extracted energy is directly linked to the vibration amplitude of the objects. A smaller spatial footprint of the system is more advantageous for designing an energy harvesting mechanism, which enhances the system's overall effectiveness. The Vibration per Swept Area (VSA) statistic is introduced in (4) to enhance the comparison of different configurations. This parameter offers understanding of the system's dimensions and its correlation with vibration intensity.

$$VSA = \frac{\sum_{i=1}^{n} A_i^*}{L\,W} \tag{4}$$

Where A_i^* represents the vibration amplitude of the ith object, L represents the total horizontal extent of the system, and W indicates the maximal vertical distance traversed by the objects during a single vibration cycle.

2.3 Numerical Method

This study utilizes the finite volume method to quantify the governing equations. Time aspects are divided into discrete intervals using a first-order implicit time integration method. Convection terms are handled using a second-order upwind technique, while diffusion terms are dealt with using a cell-based least square scheme for spatial discretization. The pressure-velocity coupled equations are solved using the SIMPLE technique. In addition, a diffusion-based smoothing method is used in this study coupled with a User-Defined Function created in the C Programming Language to analyze the object's response to Wake-Induced Vibration (WIV). The size of the computational area, especially the blockage effect, is crucial in numerical simulations. Choosing a region that is too small can affect the results. Transverse

vibration in Flow-Induced Vibration (FIV) models might worsen inaccuracies. Studies have shown that a computational area with a blockage of more than 2.5% around a circular cylinder could cause hysteresis in the vibration response when entering the lock-in regime. Therefore, for this research, setting lateral limits with a blockage of 2% is considered appropriate. (Prasanth et al., 2006), (Prasanth and Mittal, 2008), and (Prasanth and Mittal, 2009).

The boundary conditions are specified in Figure 2. The center of the cylinder is set as the origin of the coordinate system, and the rectangular computing domain spans 75D×50D. The upstream and lateral limits are located at a distance of 25D from the center of the cylinder, while the downstream boundary is set at 50D from the origin to prevent computational errors.

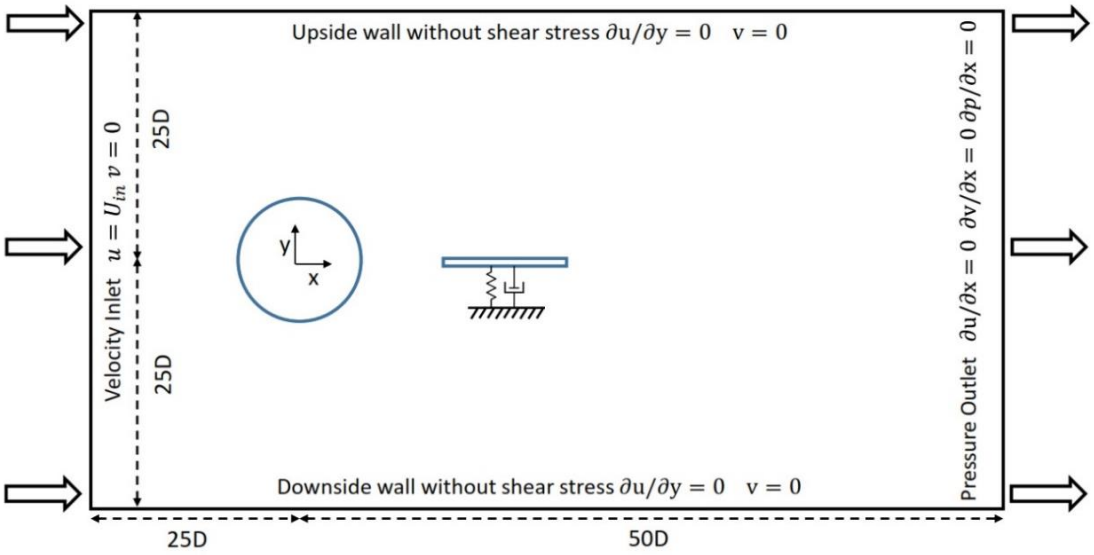

FIG. 2) Computational domain and boundary conditions

The inlet boundary condition is under a uniform velocity condition ($u = U_{in}$,$v = 0$). The velocity at the outflow has a predetermined zero normal gradient, and the pressure is set as the reference value of zero. The boundaries are defined by the normal velocity component, where the stress vector component parallel to the boundary is zero ($\partial u/\partial y = 0, v = 0$). Both the cylinder and the plate(s) have a no-slip condition applied to their surfaces.

2.4 Method validation

Prior to thoroughly examining the main cases, it is crucial to perform a grid independence study and validate the numerical methods. Two specific situations are selected to verify the accuracy of the procedure. The first scenario deals with the natural oscillation of a single flat plate positioned behind a circular cylinder, whereas the second scenario features two parallel flat plates mounted in the wake and immobile. Therefore, two distinct grids are built, as seen in Figure 3.

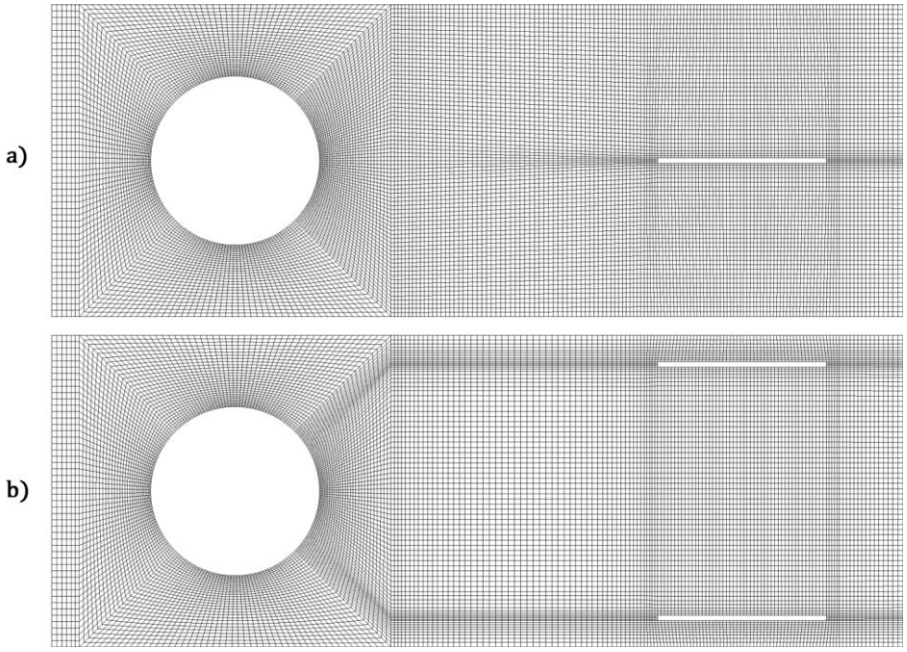

FIG. 3) Grid distribution. a) Single Plate b) Parallel Plates.

The cylinder's surface in both grids is divided into four distinct sections: front, top, bottom, and rear sides. The rear side is especially significant because of the increased flow gradients in the nearby wake zone. The use of flat plates in this location increases the complexity of the flow dynamics in that specific region. As a result, the grids are made more detailed in specific zones and surrounding the entities, then gradually made less detailed in farther places to decrease processing requirements. Three grids with different mesh densities are created for each scenario to ensure grid-independent results. In both cases, the cylinder upstream does

not move, while the plate(s) downstream are allowed to vibrate freely in the direction of the crossflow. Tables I and II provide the root mean square lift coefficient, CL_{rms}, and mean drag coefficient, CD_{mean}, for the cylinder with maximum vibration amplitude, as well as the CL_{rms} for the plate(s).

TABLE I) Grid dependency study (G=2–H=0, Single plate)

Grid	Cylinder Nodes	Cylinder		Single Flat Plate	
		CL_{rms}	CD_{mean}	A^*_{max}	CL_{rms}
SP-1	180+70	0.069	1.18	0.28	0.267
SP-2	180+80	0.073 (5.8%)	1.194 (1.2%)	0.282 (0.7%)	0.273 (2.2%)
SP-3	180+90	0.075 (2.7%)	1.199 (0.4%)	0.281 (0.35%)	0.274 (0.3%)

Increasing the number of cells on the back side of the cylinder improves the accuracy of predicting hydrodynamic parameters for both the plate and the cylinder, particularly the CL_{rms} of the cylinder. The results show that the increased mesh density of grid SP-2, with 33% more nodes on the back of the cylinder along the wake, confirms its effectiveness in predicting accurately.

TABLE II) Grid dependency study (G=3-H=1, parallel plates)

Grid	Cylinder Nodes	Cylinder		Parallel Flat Plate(s)	
		CL_{rms}	CD_{mean}	A^*_{max}	CL_{rms}
PP-1	180+80	0.24	1.297	0.356	0.38
PP-2	180+90	0.249 (3.75%)	1.30 (0.3%)	0.36	0.386
PP-3	180+100	0.253 (1.6%)	1.30 (0%)	0.36	0.389

When using parallel plates, results from grid PP-2 show that adding 50% extra cells to the rear side of the grid ensures that the results are not affected by the grid resolution. Both grids were analyzed at different time intervals for temporal resolution, with a non-dimensional time step of $\Delta t = 0.002$ ($t_{Non-D} = tU/D$ found to be sufficiently small to guarantee independence, as demonstrated in Table III.

Table III) Time step dependency study for single and parallel plates

Grid	Time Step	Flat Plate Amplitude	
		G=3-H=0	G=3-H=1
Single Plate	0.004	0.54	0.351
	0.002	0.515	0.32
	0.001	0.51	0.314
		G=3-H=1	G=4-H=1
Parallel Plates	0.004	0.377	0.389
	0.002	0.36	0.384
	0.001	0.35	0.382

As stated earlier, to establish a validated computational method requires investigating two distinct cases. The first case aims to confirm the effectiveness of the method in simulating the flow dynamics around a cylinder and a single flat plate, while the second case concentrates on parallel plates. Jebelli and Masdari (2022) examined the Flow-Induced Vibration (FIV) of a single flat plate positioned along the central axis of the wake in their previous study. Therefore, a similar approach is used in this study for setups that include a single flat plate. The mean drag coefficient of a cylinder with two parallel flat plates installed in the wake is modeled and compared in the second case, as shown in Figure 4.

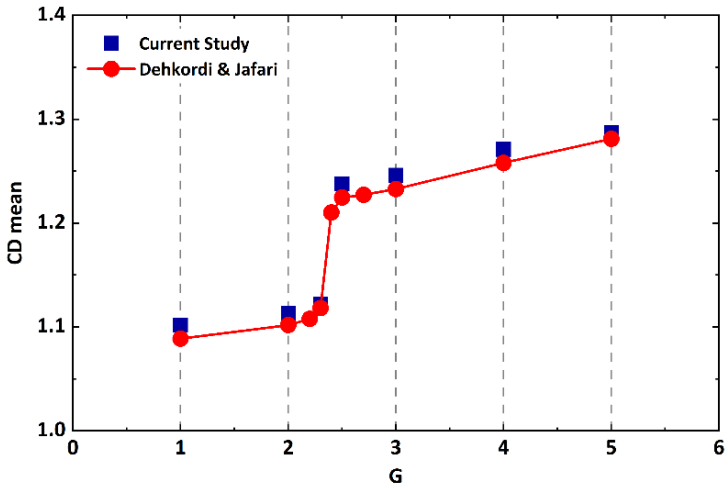

FIG. 4) Numerical method validation for fixed cylinder and parallel plates. (Dehkordi and Jafari, 2010)

The flat plates are positioned at a vertical distance of 0.75H from the horizontal axis. Upon reviewing the results, the reduction of the gap leads to a slow decrease in the Cd_{mean}. When the gap reaches a magnitude of G = 2.3, the mean drag experiences a significant decrease, followed by a slight reduction for smaller gaps. The little differences in results support the accuracy of the numerical method in predicting the flow dynamics between entities and the impact of downstream plates on the upstream cylinder. The numerical methodology used demonstrates a high level of accuracy in simulating Flow-Induced Vibration (FIV) for either a single downstream flat plate or two parallel plates.

3 Results and discussions

This section explains the details of Flow-Induced Vibration (FIV) on downstream single or parallel flat plates. Initial simulations were conducted under different setups at a lower speed of 6, where the natural frequency of the plate(s) downstream matched the vortex shedding frequency of the cylinder upstream. The results are divided into three separate subsections to enhance clarity and promote better comprehension. The first paragraph describes the behavior of a single plate (Section 3.1), covering the vibration amplitude, applied forces, and wake structure in various setups. It also outlines the response patterns for cases with high amplitudes. The following part describes the results for the parallel plates in a consistent way (part 3.2). A comparison analysis is conducted to determine the potential effectiveness of the system in developing an energy harvesting mechanism (Section 3.3).

3.1 WIV of a single wake-mounted flat plate

This section delves into the study of Flow-Induced Vibration (FIV) of a single flat plate, examining various configurations consisting of eight horizontal and five vertical locations. The analysis involves a thorough evaluation of vibration amplitude and hydrodynamic forces, as well as an investigation of wake structure using pressure coefficient, vorticity, and streamline contours. The study then focuses more on cases with large amplitudes by including a range of lower velocities.

3.1.1 Vibration amplitude and hydrodynamic forces

The vibration amplitude of the single flat plate in various horizontal and vertical positions is illustrated in FIG. 5. As the lift force is usually the main source of energy for transverse vibration, the root mean square values of lift coefficient (CL_{rms}) are also presented for both objects. According to the results, the plate's response can be divided into two distinct parts based on its amplitude, determined by a critical horizontal position of G=3.

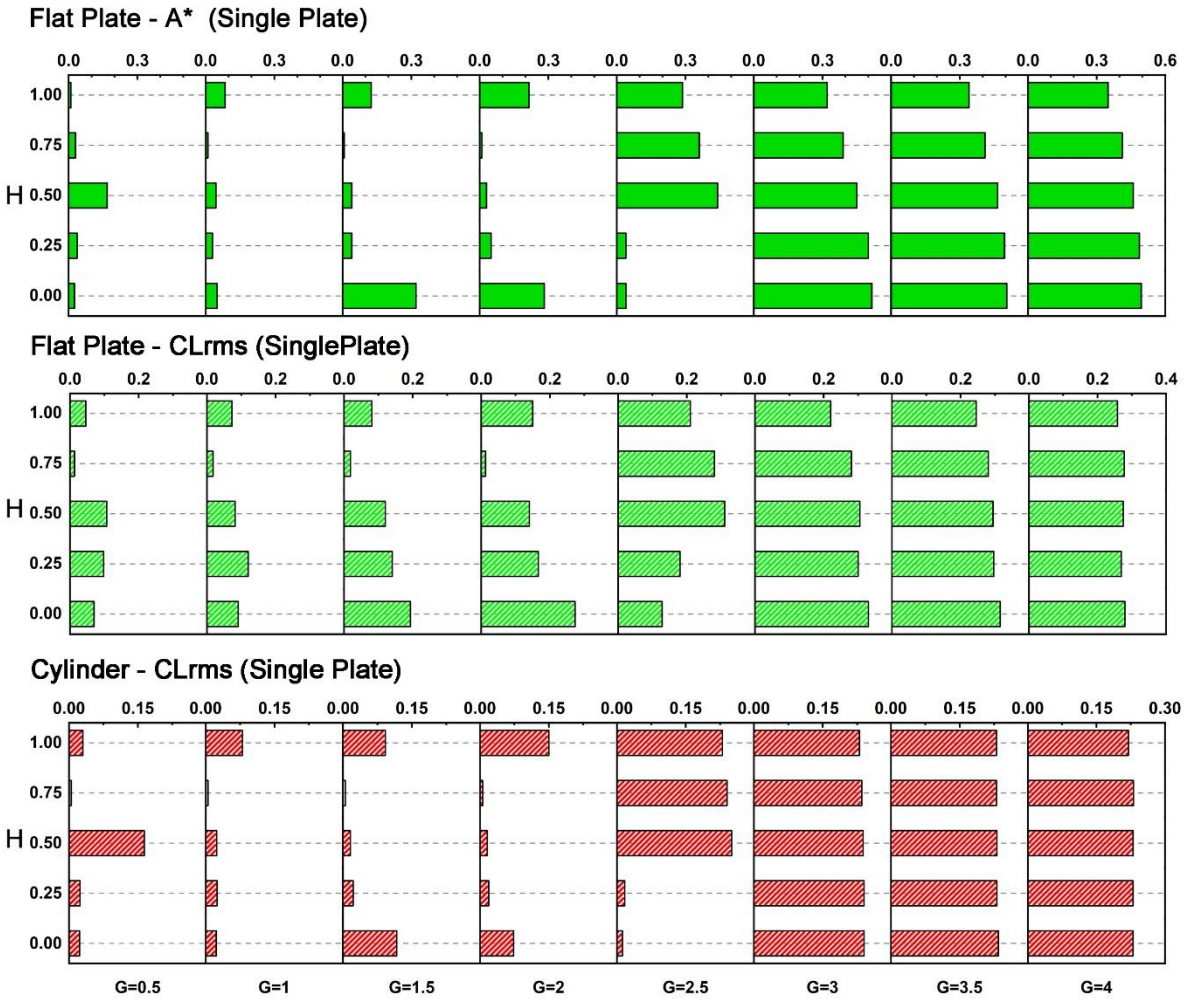

277 **FIG. 5) Vibration amplitude and CL_{rms} of the single flat plate and the cylinder in different configurations at Ur=6**

278 When the plate is mounted at horizontal distances of G≥3, it causes oscillations at all vertical
279 positions with a significant amplitude. The highest point of A* occurs when the plate is in line
280 with the center axis of the wake (H=0). When the vibration moves away from the central
281 point, the amplitude decreases gradually until it reaches its lowest point at H=1. Conversely,
282 when the horizontal spacing is less than 3 (G<3), the plate shows a significant reliance on its
283 placement. At G=2.5, there is minimal vibration at H=0. However, vertical separations greater
284 than 0.25 cause a sudden increase in amplitude at H=0.5, followed by a gradual decrease. The
285 amplitude is typically low and may be regarded insignificant for most designs across short
286 horizontal intervals, except for G=1.5, 2. The horizontal positions are linked to moderate and
287 somewhat reduced amplitudes at H=0 and 1, respectively. For the highest vertical separation

(H=1), the plate vibrates over a wider range of horizontal distances, reaching up to G=1.5. This indicates the possible existence of a different vibratory mechanism, which will be further investigated in the following section.

The variation of lift for the cylinder shows that placing the flat plate more than 3 times the cylinder diameter away has no effect on the lift properties of the cylinder upstream, regardless of its vertical position. A noticeable relationship is seen between the amplitude A* of the plate and the root-mean-square lift coefficient (CL_{rms}) of the cylinder when the horizontal gap is limited. At G=2.5, there is a minimal increase in lift at H=0 and 0.25, but substantially higher values are observed at higher vertical positions. The CL_{rms} of the cylinder increases at narrower gaps, especially when the flat plate shows significant amplitude. A significant coefficient of lift is observed for the flat plate when placed at G≥3. At these levels, the lift slightly decreases as the plate is moved to higher vertical locations. Examination of setups with a G factor of 2.5 shows that the highest lift is reached at a height of 2.5, corresponding to the increase in vibrational magnitude. Instances with G values of 1.5 and 2 exhibit similar patterns, showing increased lift at H=0 that decreases at higher vertical locations and becomes insignificant at H=0.75, before increasing again at H=1. With smaller horizontal distances, the CL_{rms} often stays relatively low.

The impact of the moving flat plate on the flow patterns behind the cylinder is also evident in the average drag force. For G≥3, the plate has minimal effect on the cylinder, as seen in FIG. 6. An increase in the mean drag coefficient is noticed for the cylinder at G=2.5-H=0.5, however at closer horizontal positions, the flat plate mostly causes a decrease in the drag force on the cylinder.

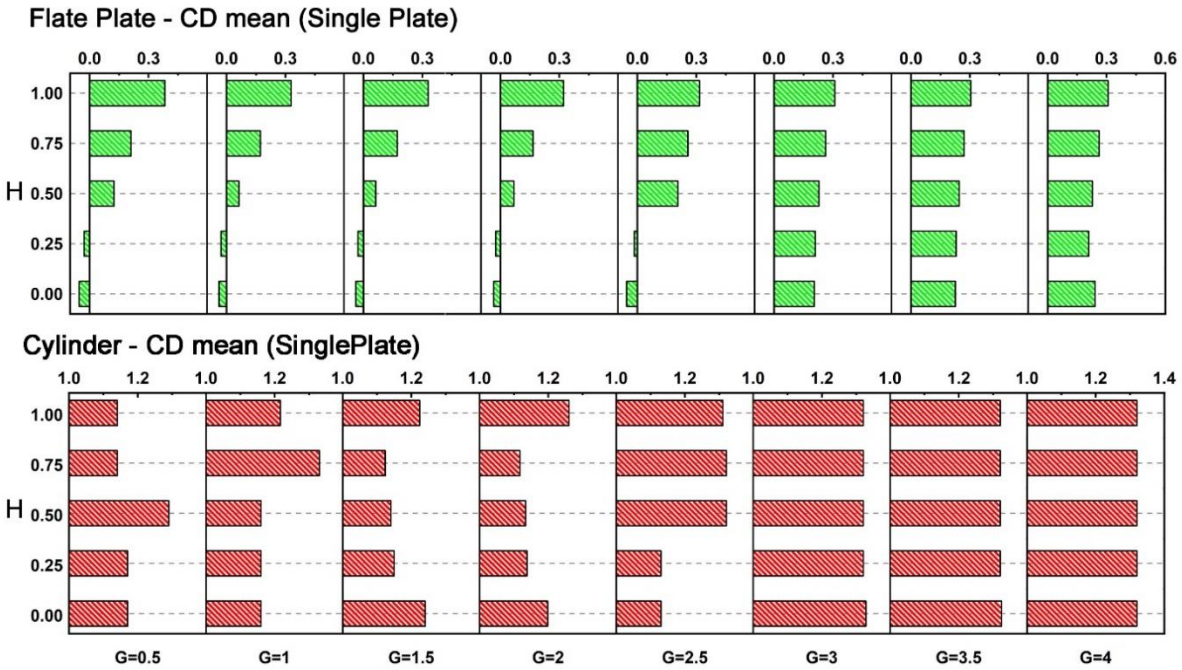

FIG. 6) Mean values of drag coefficient for the cylinder and single flat plate in different configurations at Ur=6

The drag coefficient mean of the flat plate increases as it moves away from the wake centerline at all horizontal intervals. While the increase in rate is considered low for G≥3, it becomes more noticeable in smaller gaps, showing a decrease in average drag at H=0, 0.25. This suggests possible changes in flow patterns with adjustments in vertical placement.

Examining the lift and drag coefficients confirms the previous claim that a horizontal separation of G=3 is a crucial boundary. Oscillation occurs inside this boundary, regardless of vertical alignment, and has minimal impact on the lift and drag forces of the upstream cylinder.

3.1.2 Wake Structure and vibration mechanism

The system's response can be divided into four separate parts depending on the plate's amplitude, as outlined in TABLE IV. The first segment includes situations where the plate is attached at G=0.5, 1, showing modest or insignificant amplitudes. The following section includes cases with G values of 1.5 and 2, where significantly high amplitudes are recorded

when the plate is located at heights of 0 and 1. At G=2.5, there is a noticeable increase in A* at H=0.5. The section from G=3-4 demonstrates consistently high A* values at all elevations.

TABLE IV) The system response of a single plate categorized by vibration amplitude.

Horizontal Distance	Main Characteristics
G= 0.5, 1	Small A* regardless of H
G= 1.5, 2	Relatively large A* at H=0, 1
G= 2.5	Sudden jump in A* at H=0.5
G= 3, 3.5,4	Large A* regardless of H

Instantaneous non-dimensional vorticity contours are illustrated at the moment when the plate reaches the highest point of its vibratory cycle to thoroughly analyze the flow dynamics in each section. FIG. 7 shows the wake arrangement for G values of 0.5, 2, 2.5, and 4, representing examples for each segment.

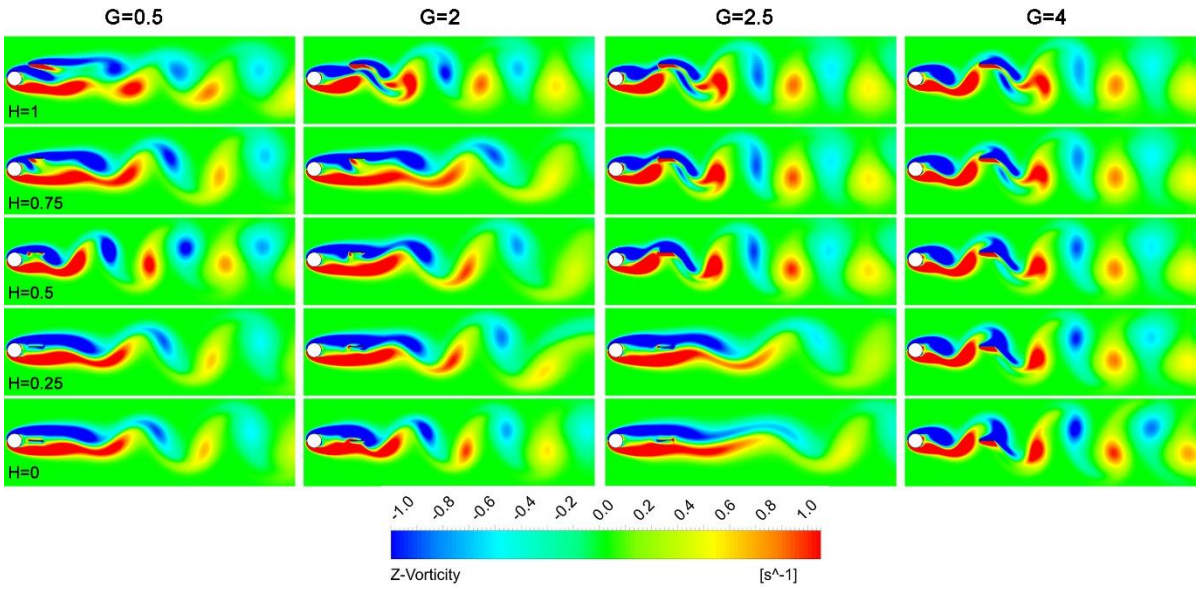

FIG. 7) The wake structure for all configurations with G=0.5, 2, 2.5, 4

In the case with G=0.5, a consistent pattern is shown for H=0 and 0.25. The flat plate causes the creation of elongated and distinct shear layers, similar to a stationary splitter. This configuration delays the start of vortex shedding to a location further downstream, resulting in a lower frequency and confirming the minimum values of CL_{rms} for the objects in question.

This wake arrangement provides additional evidence for the small values of CDmean. When the flat plate is raised to a higher vertical position at G=0.5-H=0.5, vortex shedding begins at the trailing edge of the plate. The vortex cores are closer together on a horizontal level, causing a greater change in lift. This results in a higher frequency and, as a result, a larger vibration amplitude for the plate. When the flat plate is moved to H=0.75, a different wake structure is revealed, with the upper shear layer splitting into two segments. The proximal portion interacts with the lower shear layer, while the distal segment of the upper layer, along with the lower one, delays vortex shedding further downstream, similar to the conditions seen in the H=0, 0.25 cases. At the maximum vertical distance (H=1), the splitting of the upper shear layer is clearly visible, with a larger proximal section. In these last two setups, the flat plate is mainly located inside or even beyond the boundaries of the upper shear layer, facing a flow with increased velocity and energy, resulting in a higher mean drag coefficient.

When the flat plate is positioned along the central axis of the wake (H=0) in the second case (G=2), the shear layers converge near the end of the plate, leading to the initiation of vortex shedding. This design is similar to the one seen at G=0.5-H=0.5. The following interaction increases lift fluctuations at a frequency close to the natural frequency, resulting in a rise in vibration amplitude. Further explanation of this phenomenon may be found in the author's previous study (Jebelli and Masdari, 2022). Increasing the vertical spacing to H=0.25 or 0.5 causes elongated shear layers to reappear, with the flat plate acting as a splitter. The upper shear layer bifurcates when H=0.75, but at H=1, a different flow dynamic occurs. A larger portion of the upper shear layer consistently divides, leading to an earlier start of vortex shedding compared to G=0.5-H=1 in the nearby wake. This wake setup increases lift and drag coefficients, while also improving the vibratory sensitivity of the plate.

The flow dynamics at G=2.5 require significant attention, especially because of the critical point at G=2.5-H=0.5. When H=0.25, two elongated shear layers reappear, and vortex shedding is delayed with a significantly lower frequency. Placing the flat plate at the crucial point of H=0.5 results in a significant change in the wake pattern, leading to the initiation of vortex shedding between the two objects. This modification enhances the periodic flow setup, increasing the CL_{rms} and average drag on both objects, and amplifying the plate's vibrational reaction. Moving the flat plate to higher vertical positions (H=0.75, 1) results in a matching wake formation. However, when the distance increases between the plate's location and the central axis of the wake, the plate's interaction mostly focuses on the vortices coming from the top shear layer.

Placing the plate with a significant horizontal distance (G=4) creates enough space between the objects, which helps the shear layers interact and leads to the shedding of vortices at various vertical positions. In such configurations, the impact of the plate on the cylinder located upstream is negligible, resulting in nearly identical lift and drag forces. An increase in vertical separation results in a gradual rise in drag and a corresponding decline in lift forces for the flat plate. The impact of the upper vortex becomes more noticeable as the altitude of H increases. Figure 8 displays pressure coefficient contours, lift coefficient fluctuations, and dominant frequencies for a single vibratory cycle at G=4-H=0, 0.5, 1.

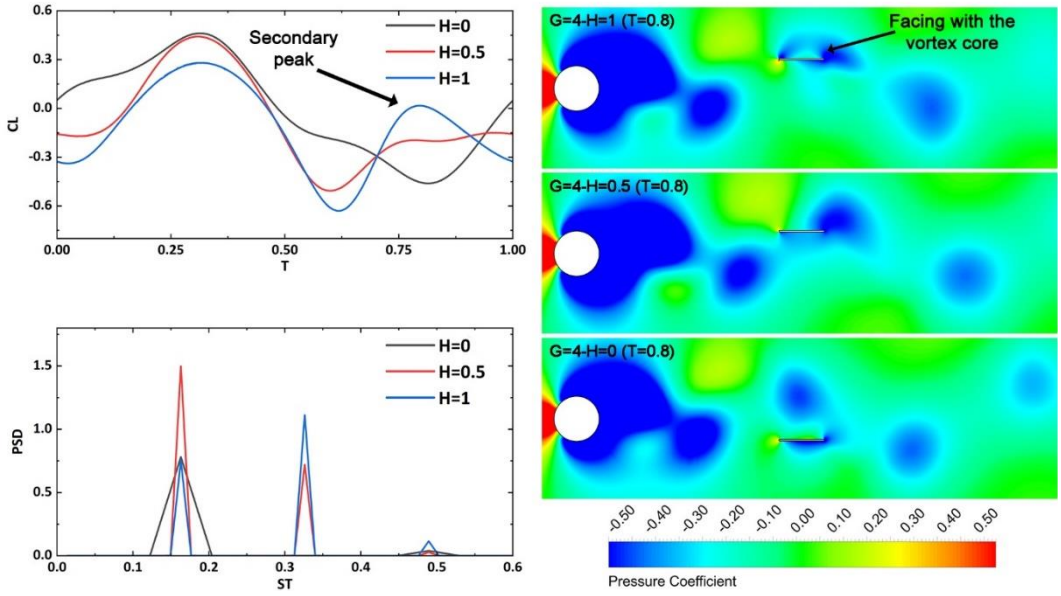

377 **FIG. 8) Variation of lift coefficient, dominant frequencies and pressure coefficient contours for G=4-H=0, 0.5, 1**

378 At H=0, a unique frequency corresponding to the vortex shedding frequency of the cylinder is
379 observed. As the plate's vertical position increases, a secondary frequency, twice the initial
380 one, appears and grows stronger. At H=0.5, the primary frequency stays the same, but when
381 the plate is mounted at H=1, the secondary frequency takes over. This phenomenon is also
382 seen in the lift variation, where a secondary peak appears during one vibratory cycle. Studying
383 the pressure coefficient contours at T=0.8 reveals the differences and origin of the secondary
384 frequency.

385 During one complete vibration cycle at H=0, the plate does not interact with the vortex cores
386 directly. Each vortex passes by while the plate is at the furthest point of its vibrating range.
387 By increasing the vertical spacing to H=1, the shedding vortex from the higher shear layer
388 meets the plate at a point where the central mounting and vibrational amplitude prevent the
389 plate from moving down enough to avoid a direct collision with the vortex. As a result, a low-
390 pressure area forms above the plate, leading to a higher lift coefficient compared to what is
391 seen at ground level (H=0).

3.1.3 Response Branch

The main goal of this study is to analyze various configurations related to Wake-Induced Vibration (WIV) of flat plates. The paper conducts a detailed analysis of configurations that show significant vibrational amplitudes. The instance where G=1.5 and H=0, showing a large amplitude (A*) with a small horizontal separation, is described as the first case. The scenario with the greatest separation and significant amplitude, while not affecting the upstream cylinder (G=4-H=0), is chosen for further analysis. Figure 9 explains the results related to G=1.5-H=0, which have been expanded to include a range of lower speeds.

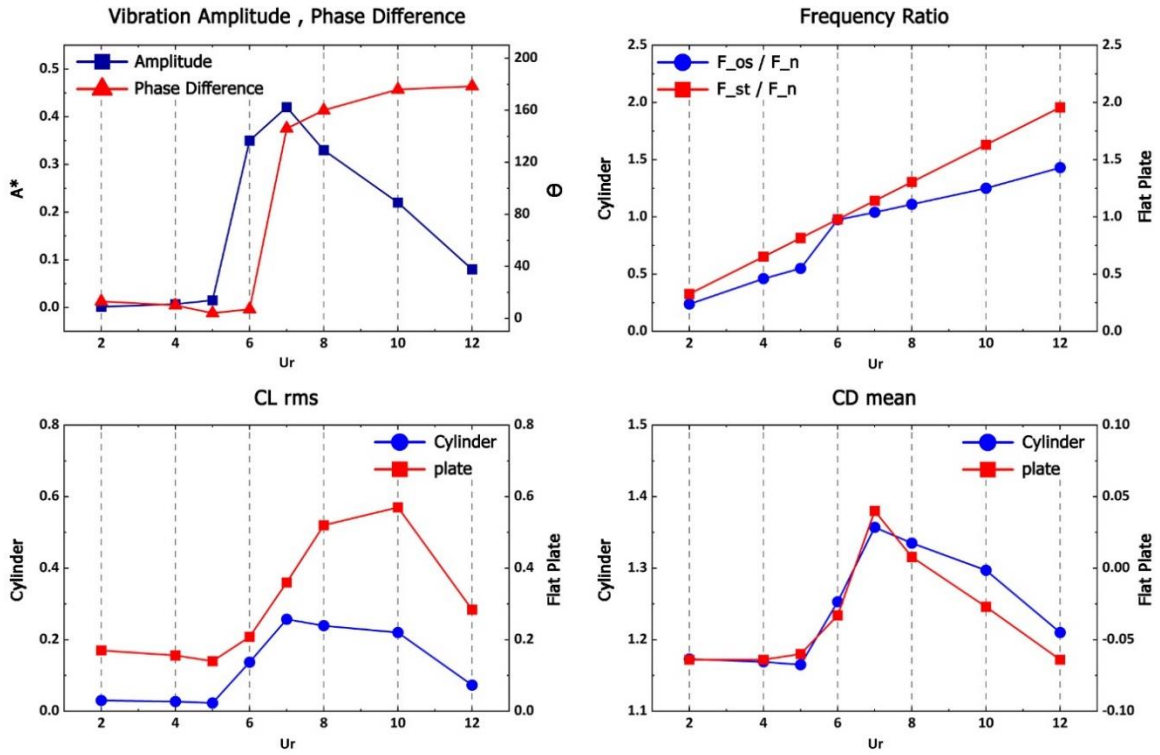

FIG. 9) WIV of the single flat plate at G=1.5-H=0 in a range of reduced velocities

The experiment shows that the vibration amplitude stays insignificant throughout the restricted velocity range of Ur=2-5. As the lowered velocity increases, there is a significant increase in amplitude, reaching its peak at Ur=7. The vibratory response decreases linearly till reaching Ur=12. A* at Ur=12 significantly surpasses those observed at Ur=2-5. The phase disparity study shows that the plate's vibration and lift force are synchronized for Ur=2-6, with

406 a sudden change in Θ occurring at Ur=7. At high speeds, the angle Θ steadily increases,
407 approaching 180 degrees. This phase transition is similar to what is seen in Vortex-Induced
408 Vibrations (VIV) of circular cylinders, happening when the vibratory frequency exceeds the
409 natural frequency (F/Fn > 1).

410 An analysis of frequency ratios shows a gradual increase in vibration within the velocity range
411 of 2-5, although at a slower rate compared to the vortex shedding frequency of a cylinder
412 without any obstacles. At Ur=6, the vibratory frequency experiences a notable increase,
413 matching the Strouhal number (Fst). This rise in height happens simultaneously with the
414 increase in vibration amplitude of the plate. At higher decreased velocities, there is a linear
415 increase in frequency ratio, although the rate of growth is slower than that of the F_{st}. The
416 plate always reflects the vortex shedding frequency, and its presence alters both the wake
417 structure and the vortex shedding frequency of the cylinder ahead. Both the cylinder and the
418 plate show a similar trend in the lift coefficient, with an increase starting at Ur=6, stable values
419 between Ur=8-10, and a reduction at Ur=12. The average drag coefficient also shows a pattern
420 of both rise and reduction. A negative mean drag coefficient is observed for the flat plate for
421 most decreased velocities, except for Ur=7 and 8.

422 Figure 10 shows the wake creation for this particular configuration at different decreased
423 velocities when A* equals 0. The immediate vorticity patterns reveal a consistent wake
424 structure for flow velocities ranging from 2 to 5, corresponding with the vibration and lift
425 characteristics. Adding the plate delays the start of vortex shedding to a location further down
426 the stream, creating a balanced flow pattern around the objects, resulting in low CL_{rms} values.
427 This setup leads to a decrease in the average drag coefficient, with negative coefficients seen
428 for both the cylinder and the plate. Vortex shedding begins at Ur=6 at the end of the flat plate,

when the plate's inherent frequency closely aligns with the shedding frequency. Furthermore, certain interactions can be observed at this speed between the shear layers in the gap.

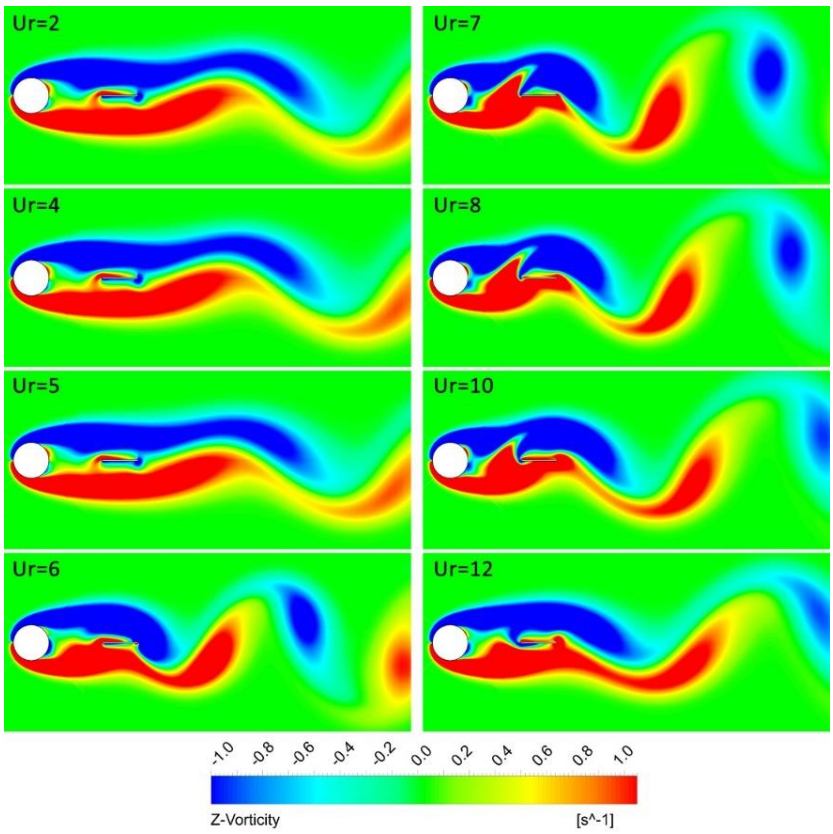

FIG. 10) Instantaneous vorticity contours in different reduced velocities for G=1.5-H=0

At Ur=7, the structure of the near-wake undergoes changes, with increased interaction between shear layers and a variation in the vortex production pattern. As the plate moves up or down, the shear layer forms nearer to the back of the cylinder. This setup helps the vortex detach from the shear layer on one side of the plate as it evolves and surrounds the other side. The maximum mean drag coefficient is observed at this velocity due to the low-pressure shear layer at the rear of the cylinder, as shown in FIG. 9. At Ur=8 and 9, the vortex production process continues but with reduced intensity. However, at Ur=10, the interaction in the wake decreases significantly, and the wake formation returns to features seen at lower reduced velocities.

FIG. 11 illustrates the temporal fluctuation of vibration amplitude and lift coefficient at Ur=6 and 7 to explain the flow dynamics for velocities with increasing amplitudes and phase shift. The vorticity, streamlines, and pressure coefficient contours are shown at T=0.25 of a vibratory cycle when the plate is at its maximum position, as illustrated in FIG. 12.

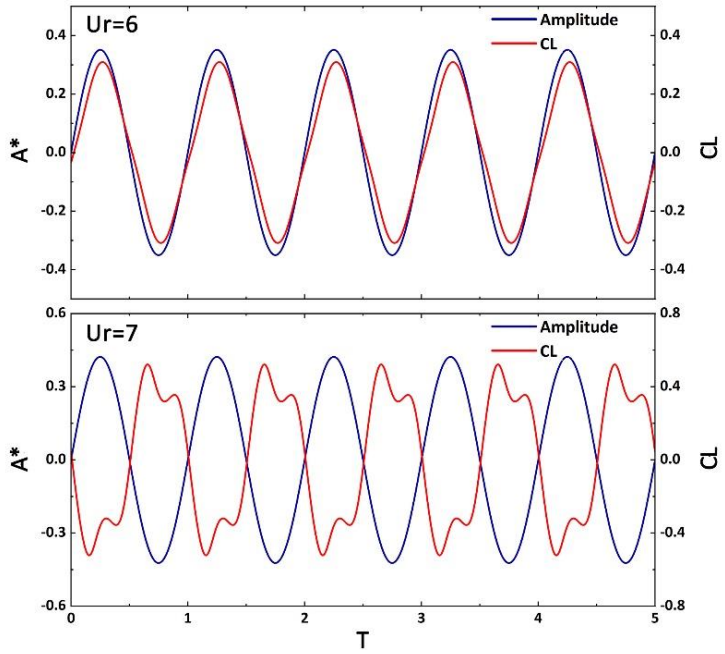

FIG. 11) Time variation of vibration amplitude and lift coefficient of the single flat plate for G=1.5-H=0

Vortices are observed to form in the near-wake structure at Ur=7, originating at the back of the cylinder. The plate's vertical movement causes the shear layer to start and develop toward the back of the cylinder, while the shear layer on the other side widens and covers the lower/upper part of the plate.

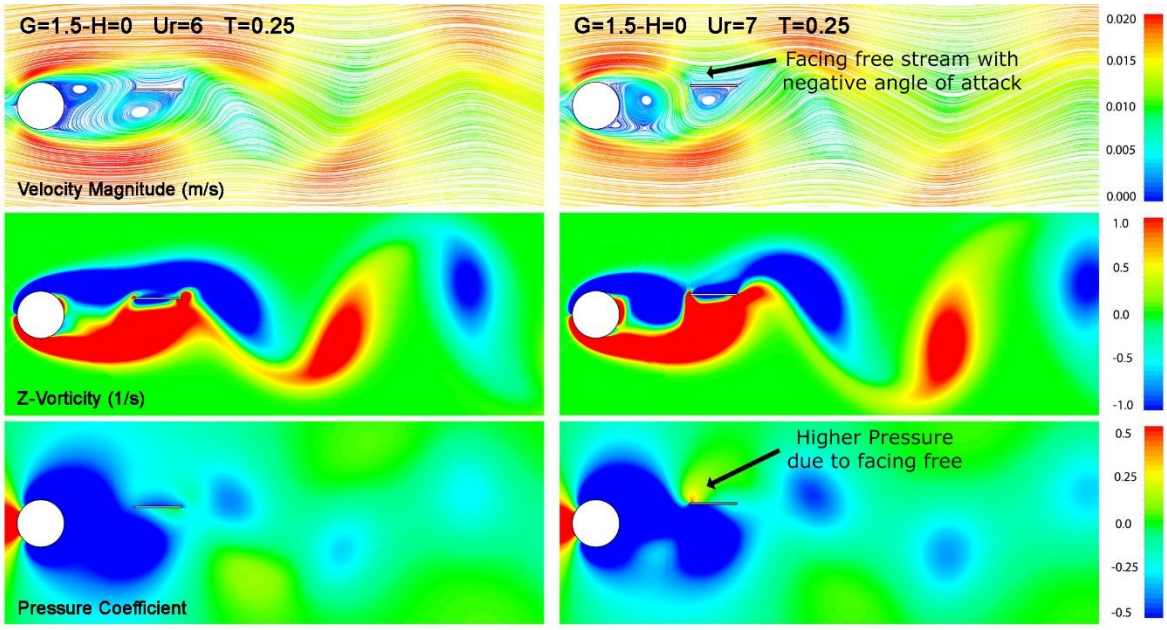

450 **FIG. 12) The vorticity, streamlines and pressure coefficient contours for G=1.5-H=0 at Ur=6, 7 (T=0.25)**

451 As the plate moves to the other side, it crosses the shear layer, causing the vortex to detach
452 and go downstream. The plate moves beyond the shear layers and is exposed to the external
453 flow at its highest points during this phase. After passing over the cylinder, the external flow
454 hits the plate at an angle, creating a high-pressure area near the front edge, resulting in a
455 downward force on the plate. This situation creates a significant difference in timing between
456 the applied force and the resulting vibration.

457

458 The vibration amplitude increases significantly as the horizontal distance extends across all
459 vertical alignments. Figure 13 illustrates the plate's response with G=4 and H=0.

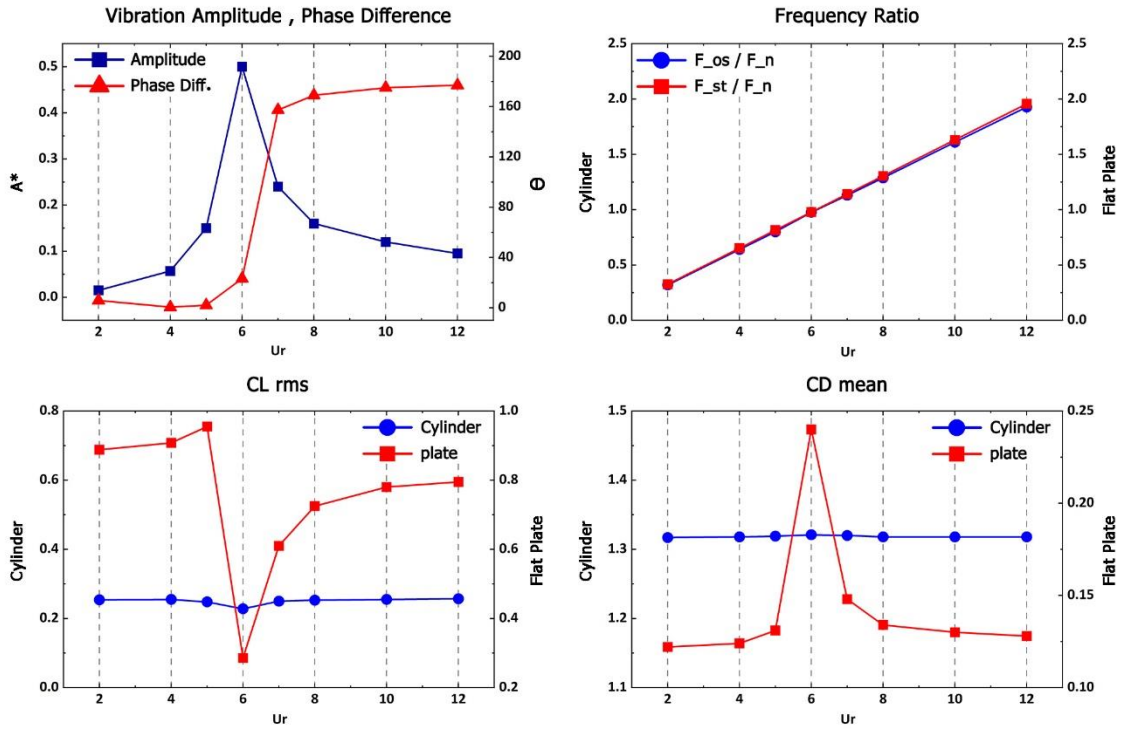

460 **FIG. 13) WIV of the single flat plate at G=4-H=0 in a range of reduced velocities**

461 The amplitude of plate vibration increases gradually as the decreased velocities range from
462 Ur=2 to 5. At Ur=6, there is a significant increase to a peak amplitude value of A*=0.5, which
463 is the highest among the other single plate setups. The amplitude decreases considerably at
464 first, then stabilizes at greater velocities. The phase difference between force and vibration is
465 similar to that seen in the G=1.5-H=0 setup, showing synchrony for Ur values between 2 and
466 5, a phase shift at Ur=7, and phase discordance at higher speeds. A sharp change in phase
467 difference occurs when F/F_n is greater than 1, similar to what happened before. The analysis
468 of frequency ratios shows that the plate consistently matches the vortex shedding frequency
469 of the upstream cylinder at all velocities examined. Furthermore, it is clear that the plate's
470 position far from the cylinder does not affect the vortex shedding frequency, unlike in earlier
471 cases. The significant increase in amplitude at Ur=6 results in a noticeable drop in lift for the
472 plate, as shown by the abrupt decline and subsequent increase in the CL_{rms} and mean drag of

the plate, respectively. The fluctuations in force confirm that the plate has little effect on the upstream cylinder, with uniform values at all lower velocities.

Positioning the plate at G=4-H=0 allows sufficient space for the shear layers to interact, as shown in FIG. 14. A consistent pattern of vortex shedding forms behind the cylinder as a result.

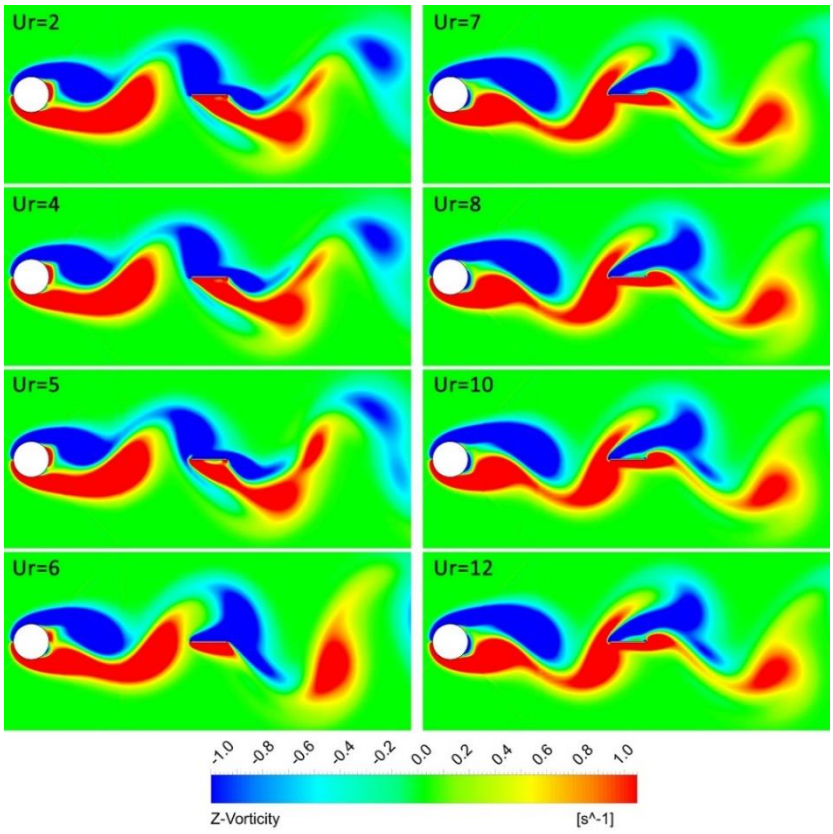

FIG. 14) Instantaneous vorticity contours in different reduced velocities for G=4-H=0

The plate interacts with oncoming vortices, which apply periodic forces, leading to the increased lift forces observed. This wake structure leads to a significant increase in the drag coefficient of the plate because it is no longer positioned between the shear layers and is directly exposed to the vortices. At Ur=6, there is a significant increase in amplitude and a decrease in CL_{rms}, followed by a phase transition at Ur=7. FIG. 15 illustrates the chronological patterns of vibration and lift coefficient for Ur=5-8, aiding in a more profound understanding of these occurrences.

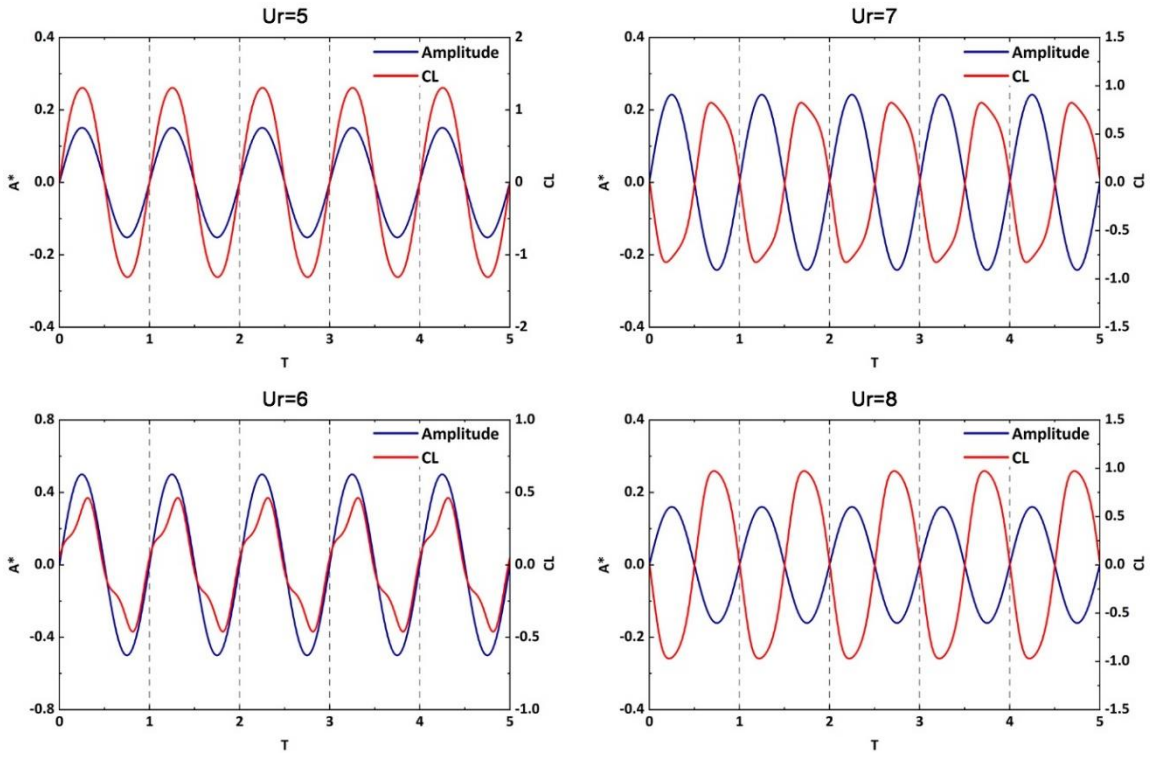

FIG. 15) Variation of vibration amplitude and lift coefficient of the single flat plate for G=4-H=0 (Ur=5-8)

The lift coefficient's behavior depends on the lowered velocity, and there is a noticeable change in the CL profile as the Ur increases. The lift coefficient displays periodic behavior in all cases, but deviates from a sinusoidal pattern at lower velocities of Ur=6 and Ur=7. This departure is most noticeable at Ur=6. An increase in Ur results in a change in the size of the phase difference. At Ur=7 and 8, the phase difference approaches around 180 degrees, while at Ur=5, it closely approximates zero. Figure 16 illustrates the wake configuration at T=0.25 to highlight the differences at Ur=6 and 7 that cause the phase shift.

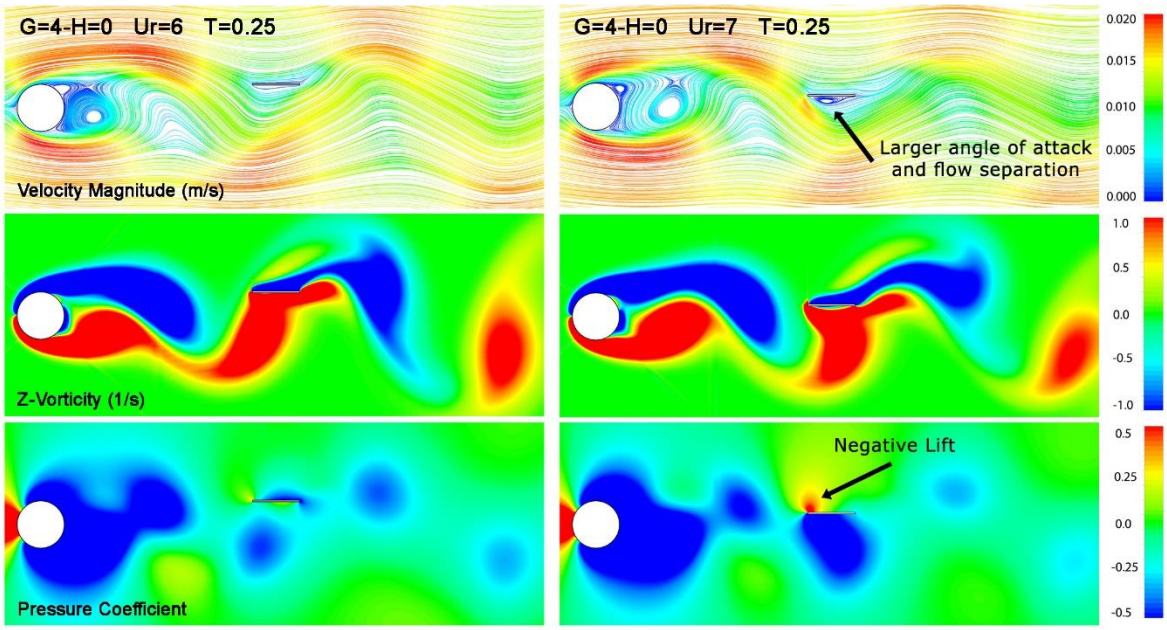

494 **FIG. 16) The vorticity, streamlines and pressure coefficient contours for G=4-H=0 at Ur=6, 7 (T=0.25)**

495 Although the wake structure is generally similar, especially in terms of vorticity, there are
496 subtle differences that explain the phase shift mentioned earlier. As shown in FIG. 13, the
497 vibration at various decreased velocities corresponds to the vortex shedding frequency
498 produced by the cylinder. Therefore, as the speed decreases, the lift force frequency deviates
499 from the natural frequency, resulting in a decrease in vibration amplitude at Ur=7. The
500 decreased maximum amplitude causes the plate to experience a higher angle of attack when
501 it encounters the external flow, resulting in higher velocity and energy, which leads to flow
502 separation on the lower side of the plate. This setup creates an increased pressure difference
503 and a stronger vertical force, directed opposite to the motion. This process explains the phase
504 difference seen at Ur=7.

505 Due to the proven effectiveness of a single plate in Wake-Induced Vibrations (WIV) regardless
506 of its position on the wake centerline, parallel plates have been selected for further
507 investigation. More information on this will be provided in the next section.

3.2 WIV of parallel wake-mounted flat plates

This part examines the Wake-Induced Vibrations (WIV) of two parallel flat plates, analyzing eight horizontal and four vertical configurations. The examination includes an analysis of the plates' vibration amplitude and hydrodynamic forces, with the results being properly reported. The research also investigates wake dynamics by analyzing pressure coefficient, vorticity, and streamline contours. The study further examines the plates' vibratory behavior and potential reaction branches in scenarios with substantial vibration amplitude, following the same approach as the previous section.

3.2.1 Vibration amplitude and hydrodynamic forces

FIG. 17 shows the vibration amplitude of the flat plates installed in parallel with the wake, as well as the change in force in the transverse direction, for all objects. The amplitude measured on the plates indicates low vibration in the nearby airflow at all vertical levels. However, significant vibrations are detected when the plates are positioned far apart both horizontally and vertically. Vertical alignments within the range of G=0.5-2 exhibit insignificant amplitudes. The zone without vibration extends from G=2.5 to 3, except for H=1, where exceptionally large amplitudes are recorded. At G=3.5, the plates start vibrating for vertical separations of H≥0.5, and choosing the maximum horizontal separation (G=4) causes vibration in all setups. An increase in the vertical distance between the plates leads to a gradual decrease in the peak amplitude, a trend also observed in setups with a single flat plate. Another important feature is the appearance of a smaller vibration-free zone that occurs at greater vertical distances, which is also noticeable in the situation with just one plate.

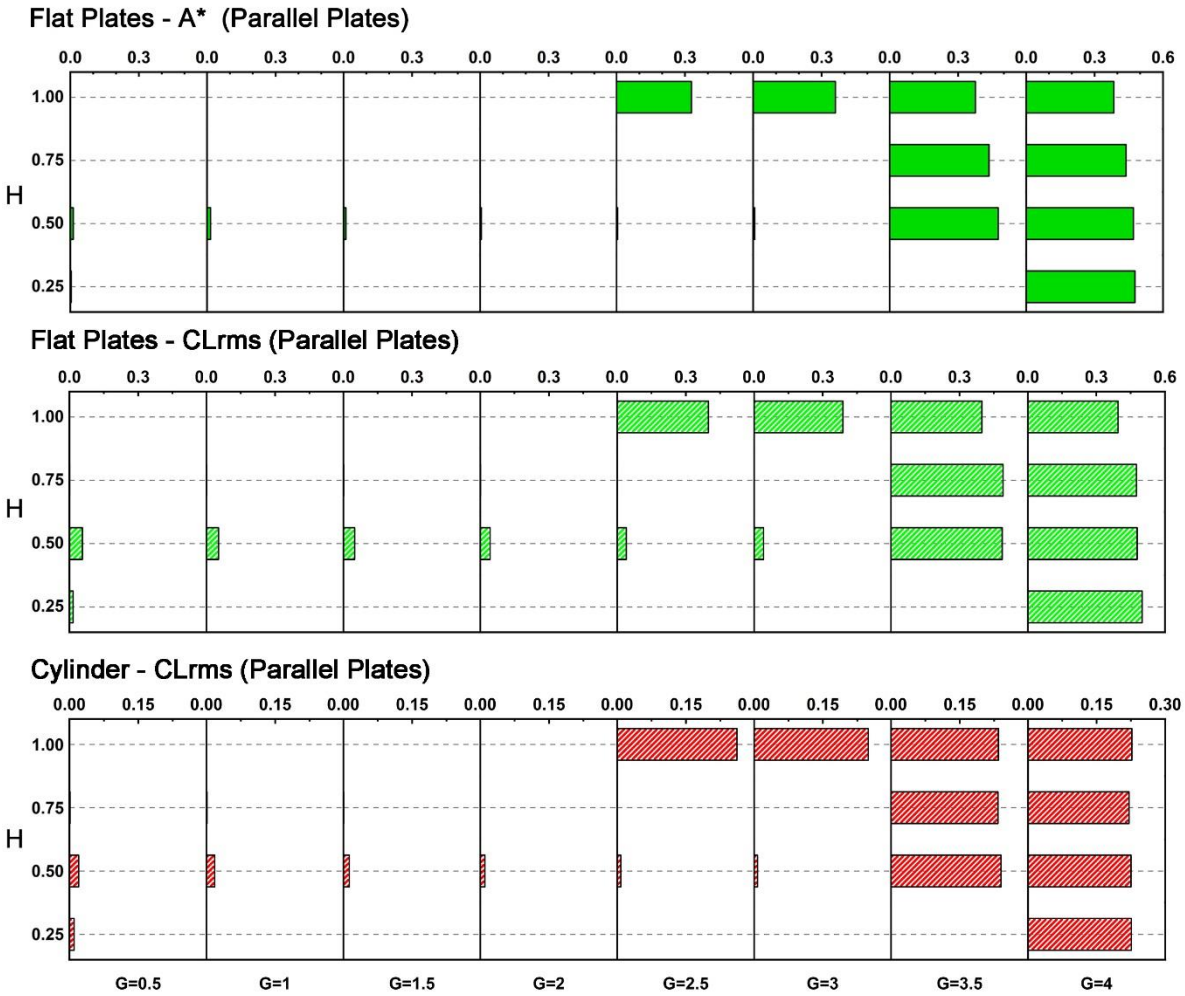

530 **FIG. 17) Vibration amplitude and CL_{rms} of the parallel flat plates and the cylinder in different configurations at Ur=6**

531 The CL_{rms} of the upstream cylinder shows correlations with the amplitude of the plates,
532 making it easier to identify areas that either show vibration or do not. In areas where the
533 plates are vibrating, the lift force on the cylinder is high and consistent, indicating that the
534 plates have no effect on it. When the plates are in equilibrium, the CL_{rms} significantly
535 decreases, indicating a form of wake flow modulation. The CL_{rms} of the plates also follows this
536 pattern, showing a gradual reduction in lift as the vertical distance increases. A little increase
537 in the lift coefficient was seen for objects located in the non-vibratory zone, particularly at a
538 vertical position of H=0.5.

The variations in the mean drag coefficient show similarities to the vibration amplitude, especially with the cylinder, but noticeable differences are also apparent, especially with the flat plates (FIG. 18). The cylinder shows a consistently even CD_{mean} when the plates are placed at appropriate distances, both horizontally and vertically. An increased average drag is noticed when the plates are located outside the non-vibratory area. On the other hand, significant decreases in CD_{mean} are observed in different setups.

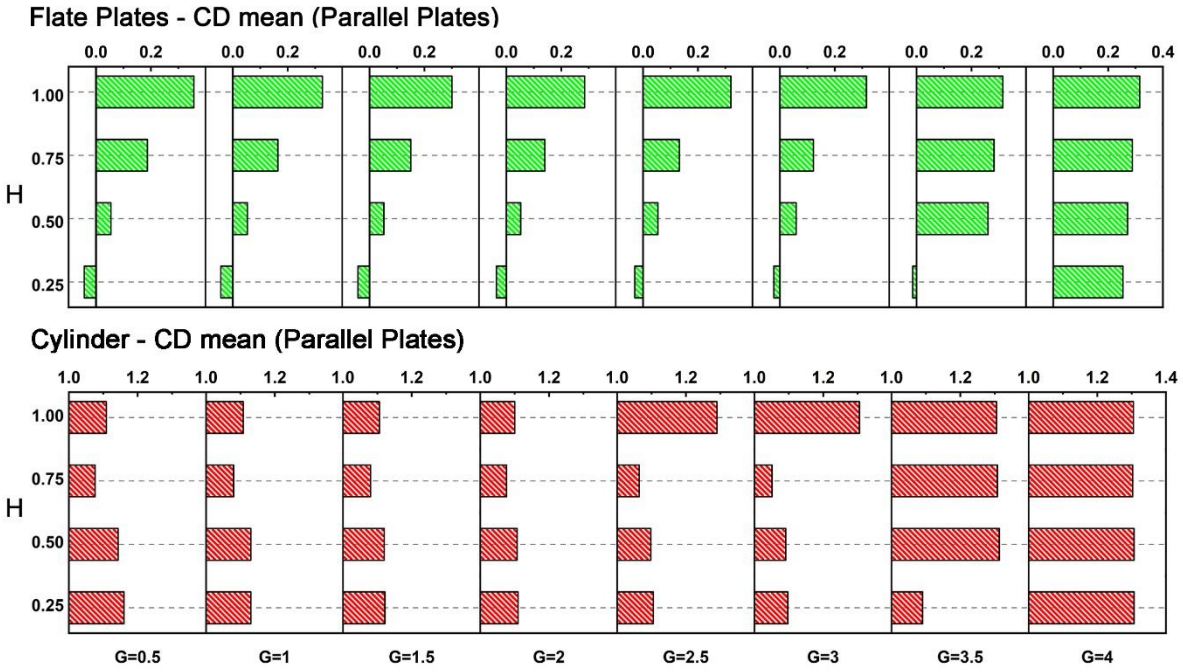

FIG. 18) Mean values of drag coefficient for the cylinder and parallel flat plates in different configurations

Flat plates have a negative average drag when positioned at the lowest vertical point (H=0.25) for most horizontal separations, except for G=4, where a higher positive value is observed. The CD_{mean} for the parallel plates mirrors the behavior seen with a single plate. When the plate(s) are located on or near the wake centerline without vibrating, a decrease in average drag is seen, and raising the plate vertically results in greater values. The CD_{mean} of the plates shows a progressive increase at G=4, unlike the sharp change from negative to significantly higher values observed in other setups (G=0.5-3.5).

3.2.2 Wake structure

Based on the findings of the previous section, the amplitude response of the parallel plates can be divided into three specific groups (TABLE V). In the first group (G=0.5-2), there is no significant vibration measured at any vertical point, indicating a controlled wake flow. In the second group (G=2.5-3), vibration starts only at H=1. Plates in the final group (G=3.5, 4) display vibratory behavior regardless of the vertical separation, except for G=3.5-H=0.25.

TABLE V) The system response of parallel plates categorized by vibration amplitude.

Horizontal Distance	Main Characteristics
G= 0.5, 1, 1.5, 2	Negligible A* regardless of H
G= 2.5, 3	Large A* only at H=0, 1
G= 3.5, 4	Large A* regardless of H

The non-dimensional vorticity contours are displayed to analyze the flow dynamics at the moment when the plates reach their vibrational midpoint. FIG. 19 shows the wake formation for G values of 0.5, 2, 3, and 4, indicating different stages of the process. Configurations with G values between 0.5 and 2 show low amplitude, and the plates remain stable. The results show that the addition of the plates causes different flow control methods, depending on the vertical distance between them. At lower intervals of H=0.25 and 0.5, the plates completely separate the shear layers. Choosing H=0.75 leads to the formation of bifurcated layers. The interior segments are concentrated in the proximal wake, while the rest are isolated and start interacting further downstream. At the highest vertical distance (H=1), bifurcated shear layers reappear, with the inner sections more prominent and the remaining parts creating two elongated, separate layers without contact.

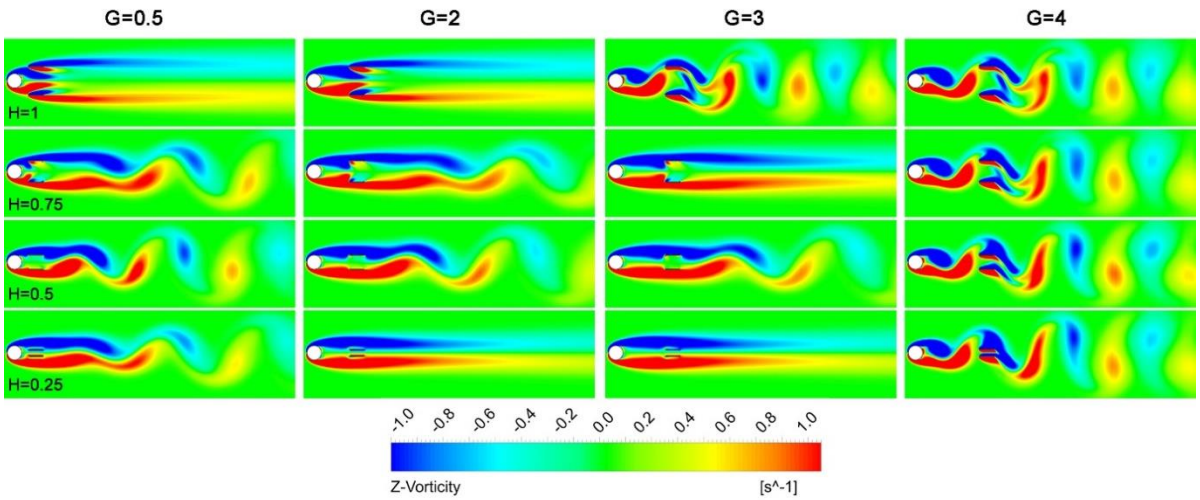

FIG. 19) The wake structure around the cylinder and parallel plates for all configurations with G=0.5, 2, 3, 4

Within the intermediate range (G=2.5, 3), the plates show stability with negligible vibration at three vertical positions (H=0.25, 0.5, 0.75), and the wake configuration closely resembles that seen in the next segment. Increasing the vertical distance to H=1 allows enough space for the shear layers to come together and merge. Therefore, the plates experience shedding vortices, creating an uneven flow field. Choosing the maximum horizontal separation (G=4) causes vibration in all vertical alignments. Vortex shedding begins in the proximal wake and in front of the parallel plates, creating an uneven flow field and causing a significant variation in the lift coefficient for all objects.

At G values between 0.5 and 3 and H value of 0.5, the CL_{rms} is slightly higher for both entities in the vibration-free zone. An analysis of the vorticity patterns in this span reveals that vortex shedding begins quite close, even though it starts later downstream in all configurations. The initial interaction with the parallel plates causes changes in the formation of shear layers, leading to more significant oscillations in the lift force.

3.2.3 Response Branch

Upon examining the amplitude response of the plates, it is noted that A* is significant regardless of the vertical separation at G=4. Therefore, two configurations, G=4-H=0.25 and

G=4-H=1, have been selected for further detailed examination, with simulations extended to include a range of lower velocities. The second part showed similarities in the development of waves in both of these environments. Therefore, the results and relevant debates will be presented simultaneously. FIG. 20 shows the results for the smaller vertical distance (H=0.25).

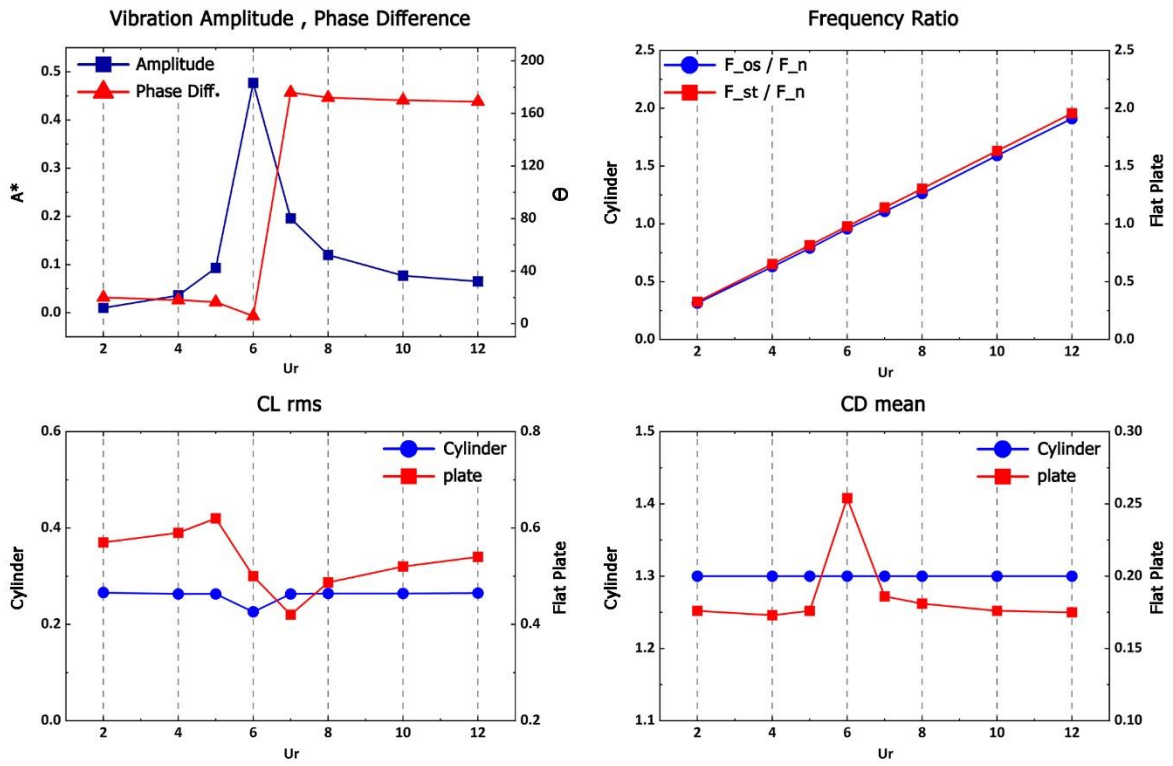

FIG. 20) FIV of the parallel flat plates for G=4-H=0.25 in a range of reduced velocities

The vibration amplitude gradually rises at progressively decreased velocities between Ur=2-5, then sharply increases to a peak value of A*=0.48 at Ur=6, which is the highest amplitude recorded in parallel plates. At higher decreased velocities, there is an initial decrease in amplitude, followed by a little reduction in A*.

At lower velocities between Ur=2 and 5, the lift force and vibration are coordinated. At Ur=7, a phase transition happens where vibrations go out of phase at high speeds. This phase change occurs repeatedly when the frequency ratio surpasses 1. The analysis of the frequency ratios shows that the plates reliably match the vortex shedding frequency of the upstream

cylinder at all reduced velocities, without appreciably affecting the wake of the cylinder. Increased vibration amplitude at Ur=6 leads to decreased lift and higher mean drag coefficient of the plates due to hydrodynamic forces. The results for the second case (G=4-H=1) are shown in the figure. 21.

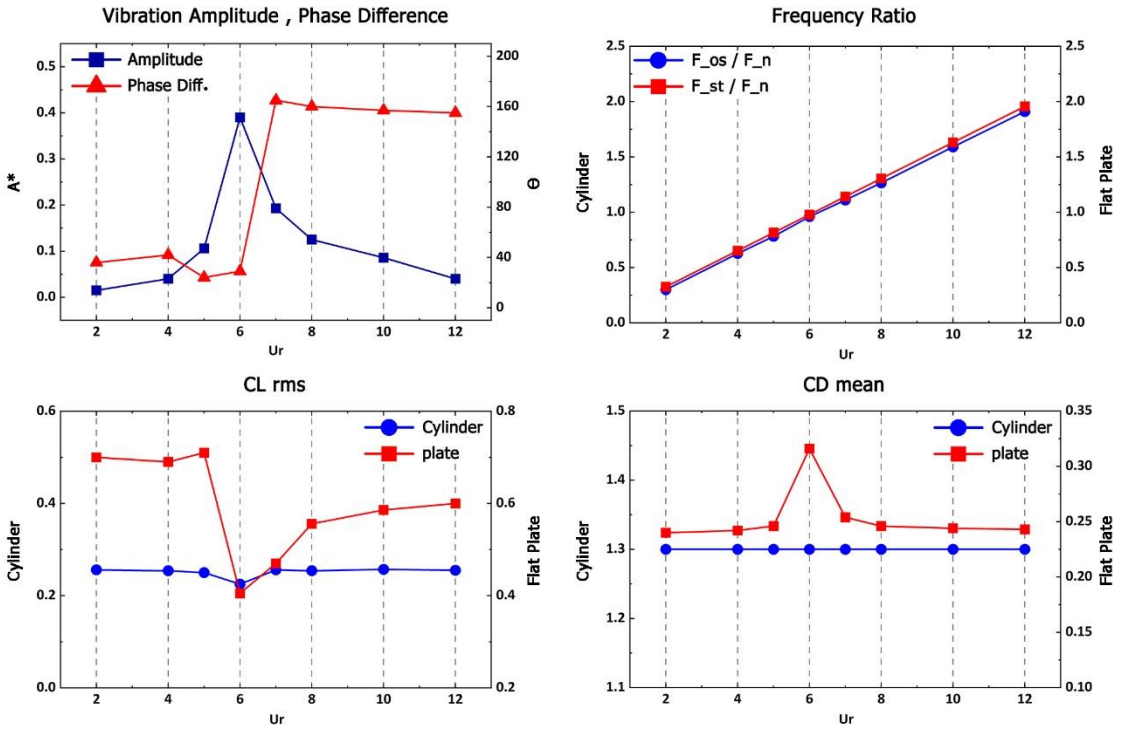

FIG. 21) FIV of the parallel flat plates for G=4-H=1 in a range of reduced velocities

In this situation, the vibration amplitude and phase difference show similar features to the previous case, with low amplitude recorded at Ur=2-5, a peak A* at Ur=6, and a gradual decrease at higher velocities. The zenith amplitude is about 0.4, lower than the value observed for H=0.25. The phase difference displays a similar pattern, with a significant change occurring at Ur=7. The parallel plates vibrate synchronously with the vortex shedding frequency of the upstream cylinder at all tested velocities. The study of hydrodynamic forces shows that the CL_{rms} and CD_{mean} of the cylinder exhibit similar trends and magnitudes, but the plates exhibit higher mean drag values when placed at H=1. The lift coefficient shows small fluctuations, with higher values observed for lower reduced velocities of Ur=2-5.

Due to the similar system responses, the wake structure is compared for both configurations in the reduced velocities around the amplitude peak (FIG. 22). The variation of lift and drag coefficient for the upper plate are also presented for five cycles of vibration at Ur=6.

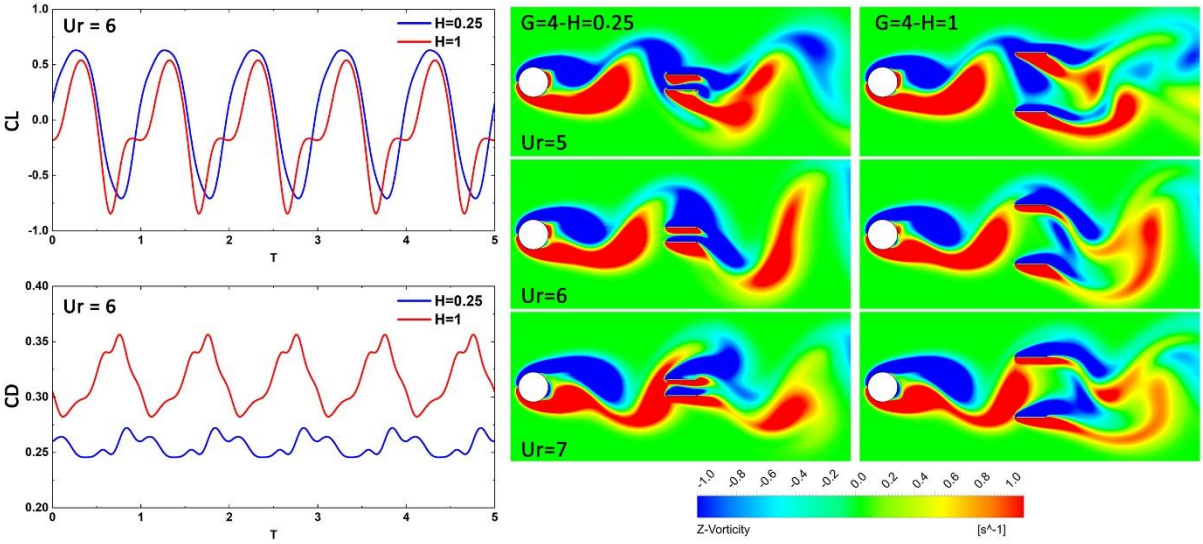

FIG. 22) Variation of lift and drag coefficient at Ur=6 and Instantaneous vorticity contours in different reduced velocities for G=4-H=0.25, 1

The wake patterns show similar features, with the plates regularly encountering the shedding vortices in each case. At Ur=7, a phase shift is detected as the plates interact with the vortex coming from the lower shear layer. During one vibratory cycle at H=1, each plate faces the vortex from its corresponding side (the top plate with the upper shear layer and vice versa), with no involvement from the other plate. When the gap is reduced to H=0.25, both plates contact with the oncoming vortices at the same time.

At H=0.25, the lift coefficient follows a sinusoidal pattern as shown in FIG. 22. However, at H=1, a secondary frequency appears, causing fluctuation in the lift coefficient. Increasing the vertical separation leads to a decrease in the average lift coefficient. The CLmean is -0.1 when the separation is increased, whereas it was 0.05 when the separation was at H=0.25. Analyzing CD_{mean} shows that a greater vertical distance results in higher average values and greater variations in the vibrating plates. Figure 23 illustrates the pressure coefficient and

streamline contours for a single vibratory cycle to better understand flow dynamics and determine the causes of these occurrences.

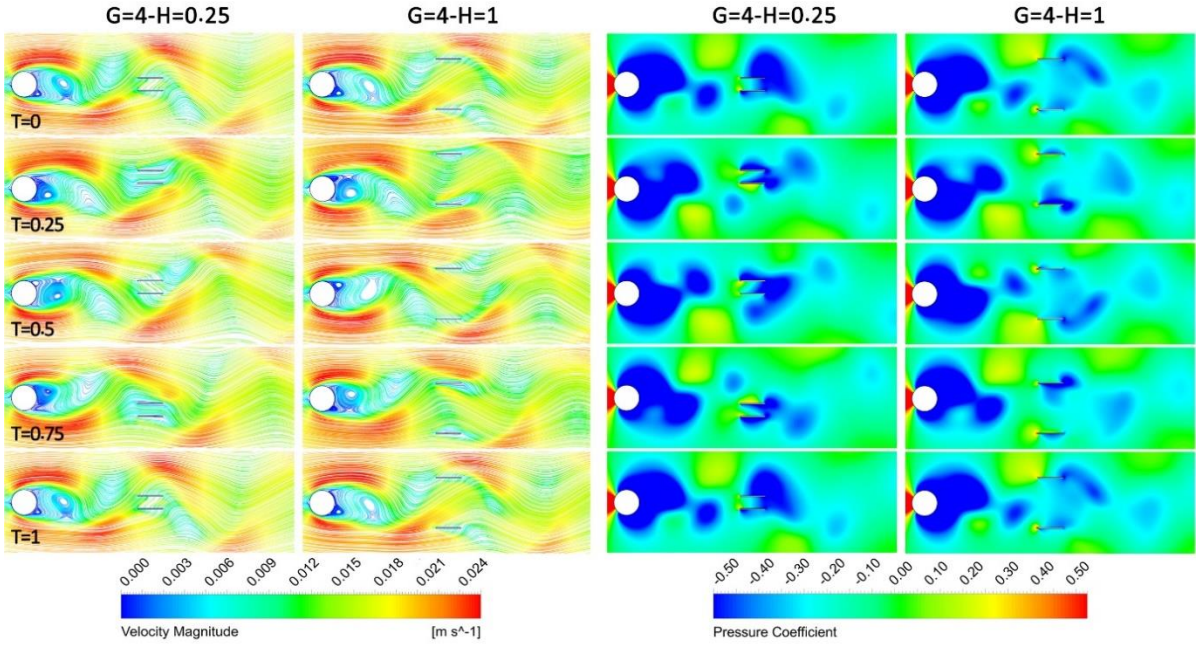

FIG. 23) Streamlines and pressure coefficient contours for one cycle of vibration for cases G=4-H=0.25, 1

An analysis of the pressure coefficient contours shows that when the parallel plates are closer to the wake centerline (H=0.25), the vortices move past the downstream objects in a periodic manner through the upper or lower sides of both plates, supporting the sinusoidal pattern seen in the lift coefficient. By increasing the vertical distance to H=1, the vortices created move through the space between the parallel plates, resulting in a low-pressure area forming surrounding each plate. This occurrence leads to the appearance of a secondary frequency, causing a disturbance in the lift coefficient, as shown in FIG. 22.

An in-depth analysis shows that the maximum amplitude decreases as the vertical spacing is changed to H=1. Two main causes are responsible for this transformation. The increased space requires the plates to interact with the external flow, which is characterized by higher energy levels. The external flow creates resistance, pushing the plates towards the centerline of the wake. The shedding vortices passing over the midway of the parallel plates apply a

centripetal force on the plates simultaneously. The combined forces result in a diverging mean lift coefficient, with a negative value for the upper plate and a positive value for the lower plate, leading to a reduction in vibratory amplitude. On the other hand, the opposite wake pattern caused by the vortices at H=0.25 results in an increased CL_{mean}, pushing the plates outward and leading to a higher vibratory intensity.

There is a significant rise in the drag coefficient in both setups when the Reynolds number is 6. At this velocity, the plates experience increased vibration amplitude due to the flow from outer layers with higher velocity. This interaction results in heightened drag forces on the plates with a Reynolds number of 6. Increasing the vertical spacing to H=1, as shown in FIG. 22, results in a higher mean drag coefficient and more fluctuations. The increased average drag can be explained by the plates' close closeness to the external layers, which amplifies the drag forces. The significant vibration amplitude leads the plates to oscillate back and forth in the wake zone, intensifying the fluctuations.

3.3 Configurations comparison

This study aims to investigate different setups for harvesting energy from the turbulent flow behind a cylinder. The total amplitude per swept area for each setup shown in FIG. 24 has been calculated using equation (4).

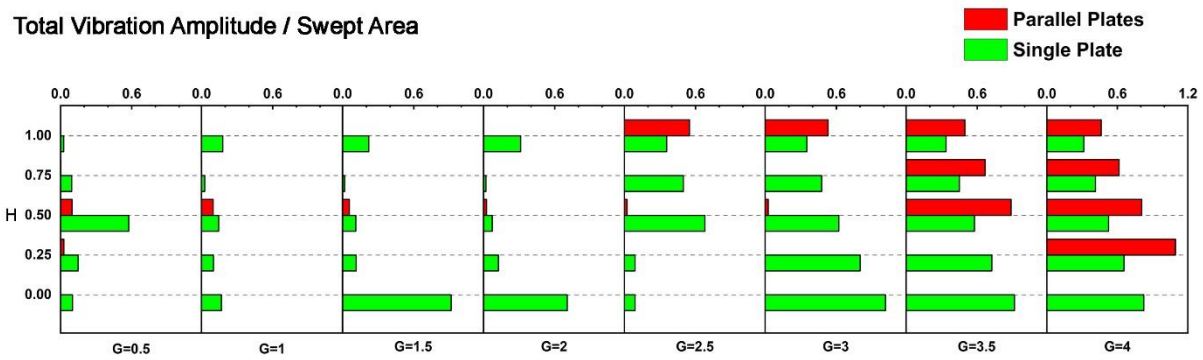

FIG. 24) Total vibration amplitude per swept area in different configurations at Ur=6

The chart being discussed shows significant similarities to the vibration amplitude shown in FIG. 5 and 17. Similar to the vibration amplitude, a significant value is consistently visible for the single plate over almost all horizontal range. At a spacing of G=0.5-H=0.5, the plate shows a notable Vibration per Swept Area (VSA) with an amplitude of A*=0.18. The narrow horizontal separation and smaller swept area lead to a high VSA, despite the amplitude not being significant. The increased values at G=1.5, 2-H=0 correspond to bigger amplitudes of A*=0.32 and 0.28 on the plate due to a similar reasoning. Positioning the plate near the wake centerline reduces the swept area, but a bigger amplitude results in much higher VSA values. A decrease in VSA is observed as the single plate's vertical alignment increases due to broader horizontal separations and expanding swept regions. The scenario G=3-H=0 exhibits the highest VSA for the single plate among all configurations, with VSA≈1.

In areas without vibration, the VSA is considered insignificant for parallel plates because of the low amplitudes. Parallel plates can demonstrate a greater Voltage Standing Wave Ratio (VSA) when the amplitude is significant, compared to similar setups with a single plate. Although these situations have lower vibratory amplitudes and greater swept areas, using independently vibrating entities results in a better VSA. Comparing single and parallel plates, it is evident that the configuration G=4-H=0.25 with parallel plates obtains the highest vibration amplitude per swept area among all configurations (VSA≈1.1).

The vibration amplitude of potential situations is thoroughly compared by assessing both maximum and average amplitudes, as shown in FIG. 25.

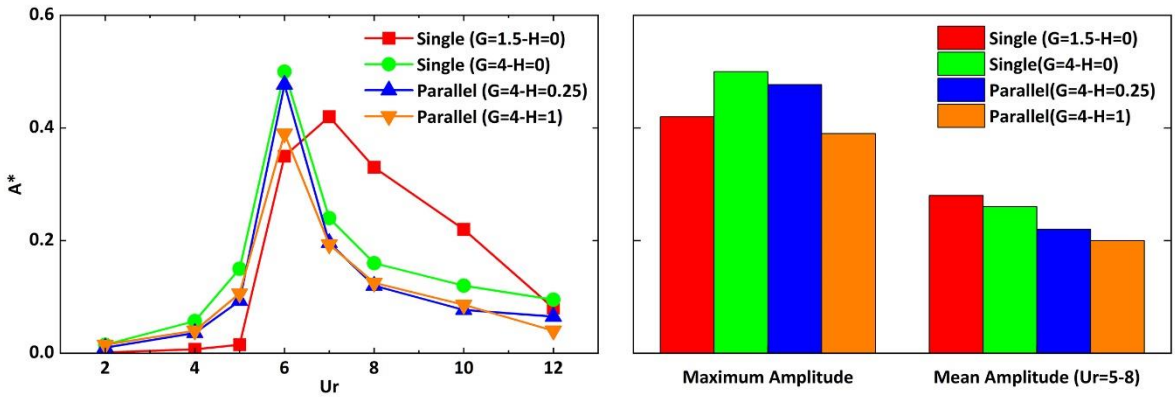

FIG. 25) Comparing the mean and maximum vibration amplitudes for cases with harvesting energy potential.

Vibration in a range of reduced velocities for the G=1.5-H=0 configuration with a single plate shows unique characteristics, reaching maximum amplitude at Ur=7 instead of Ur=6. The amplitude decreases linearly, leading to higher values of A* at lower velocities. This distinctive behavior is also evident in the highest achievable and average amplitude of the instances. While the single plate positioned at G=4-H=0 recorded the greatest A* among all configurations, the average amplitude for G=1.5-H=0 is considered to be the most significant. Ultimately, the research shows that both setups, G=1.5-H=0 (single) and G=4-H=0.25 (parallel), have significant promise for an energy harvesting system.

4 Conclusion

Numerical simulations were performed to investigate Wake-Induced Vibrations (WIV) of single or parallel flat plates, aiming to enhance understanding of vortex-plate interactions in the wake of a circular cylinder. This investigation was then widened to uncover combinations suitable to energy harvesting. Several plate configurations were examined to evaluate their impact on the upstream cylinder, expanding the analysis to cover a range of reduced velocities for specific situations. The Reynolds number, based on the free-stream velocity and the cylinder's diameter, was kept at 100. The entities had a low mass ratio of 10, and the damping effect was considered negligible (ζ=0). The study culminates in the following conclusions:

1. The examination of WIV introduces novel perspectives as a single flat plate exhibits a pronounced dependency on position within the wake of a stationary cylinder. Historically seen as a passive flow control device, the flat plate begins to show significant vibrations once it gets too close to a critical point. Elevating the plate's vertical position and distancing it from the wake centerline alters the wake dynamics and vibratory mechanism, yielding dual outcomes. A gradual reduction in the highest level of amplitude is observed, along with a shrinking of the non-vibratory area, which promotes improved mixing and interaction in the shear layer. The investigation also questions previous ideas about the plate's regulatory role in the near-wake, showing that small horizontal separations can cause vibration. These amplitudes are typically lower than those seen in wider gaps due to the unique vortex formation and flow field structure in the nearby wake. Extending the analysis to a wider velocity range shows that there is no lock-in regime, deviating from the behavior of circular cylinders. Significant amplitudes only occur when the shedding frequency is close to the natural frequency.

2. The two functions of parallel plates in the analyzed setups establish an important limit for vibratory amplitude. Across an extensive range of separations, the plates remain inert, serving as an effective flow modulation mechanism for the cylinder, manifesting two distinct actions—either separating or bifurcating the shear layers, contingent on the vertical separation. An abbreviated non-vibratory zone also materializes for parallel plates as the vertical gap widens. The vibratory mechanism itself varies with the vertical separation, encountering periodic shedding vortices at narrower gaps and confronting vortices emanating from the shear layer on the same side at wider gaps. Lock-in is not present in the chosen scenarios at different reduced velocities, but significant vibration amplitudes occur when the frequencies of vortex shedding closely match the natural frequency.

3. Comparing single plates to parallel plates in terms of vibratory amplitude and spatial occupation provides new perspectives for designing energy harvesting devices. Specifically, two distinct configurations are identified, each offering unique benefits. The first plate, positioned at G=1.5-H=0, exhibits moderate vibratory characteristics with a decreased horizontal distance and a smaller area of occupancy. On the other hand, the second configuration, with parallel plates placed at a distance downstream at G=4-H=0.25, demonstrates the benefits of using separate vibrating components.

The present study may be extended further to explore the effect of different cross-sections for the upstream cylinder to achieve higher vibration amplitudes. Additionally, future research could investigate increasing the Re number to the subcritical regime and examining the impact of changing variables such as the mass and damping ratios to examine the results under more realistic conditions.

Declaration of competing interest

The authors declare that they have no known competing financial interests or personal relationships that could have appeared to influence the work reported in this paper.

Acknowledgment

"The authors acknowledge the use of the UCL Grace High Performance Computing Facility (Kathleen@UCL), and associated support services, in the completion of this work.

References

An, X., Song, B., Tian, W., & Ma, C. (2018). Design and CFD simulations of a vortex-induced piezoelectric energy converter (VIPEC) for underwater environment. Energies, 11, 330.

Apelt, C.J., & West, G.S. (1975). The effects of wake splitter plates on bluff-body flow in the range $10^4 < Re < 5 \times 10^4$. Part 2. Journal of Fluid Mechanics, 71, 145–160.

Apelt, C.J., West, G.S., & Szewczyk, A.A. (1973). The effects of wake splitter plates on the flow past a circular cylinder in the range $10^4 < Re < 5 \times 10^4$. Journal of Fluid Mechanics, 61, 187–198.

Armandei, M., & Fernandes, A.C. (2016). Marine current energy extraction through buffeting. International Journal of Marine Energy, 14, 52–67.

Arrigan, J., Pakrashi, V., Basu, B., & Nagarajaiah, S. (2011). Control of flapwise vibrations in wind turbine blades using semi-active tuned mass dampers. Structural Control and Health Monitoring, 18, 840–851.

Assi, G.R.S., & Bearman, P.W. (2015). Transverse galloping of circular cylinders fitted with solid and slotted splitter plates. Journal of Fluids and Structures, 54, 263–280.

Assi, G.R.S., Bearman, P.W., & Kitney, N. (2009). Low drag solutions for suppressing vortex-induced vibration of circular cylinders. Journal of Fluids and Structures, 25, 666–675.

Bearman, P.W. (1984). Vortex shedding from oscillating bluff bodies. Annual Review of Fluid Mechanics, 16, 195–222.

Blevins, R.D. (1977). Flow-induced vibration. New York: Van Nostrand Reinhold Co.

Bokaian, A., & Geoola, F. (1984). Wake-induced galloping of two interfering circular cylinders. Journal of Fluid Mechanics, 146, 383–415.

Cui, G.-P., Feng, L.-H., & Hu, Y.-W. (2022). Flow-induced vibration control of a circular cylinder by using flexible and rigid splitter plates. Ocean Engineering, 249, 110939. https://doi.org/10.1016/j.oceaneng.2022.110939

Dehkordi, B.G., & Jafari, H.H. (2010). On the suppression of vortex shedding from circular cylinders using detached short splitter-plates. Journal of Fluids Engineering, 132.

772 Derakhshandeh, J.F. (2022). Analysis of wake induced vibration of a coupled circular cylinder-
773 piezoelectric using two-way fluid structural interaction. Applied Ocean Research, 121,
774 103116. https://doi.org/10.1016/j.apor.2022.103116

775 Griffin, O.M., & Ramberg, S.E. (1982). Some recent studies of vortex shedding with application
776 to marine tubulars and risers.

777 Henderson, R.D. (1997). Nonlinear dynamics and pattern formation in turbulent wake
778 transition. Journal of Fluid Mechanics, 352, 65–112.

779 Hwang, J.-Y., Yang, K.-S., & Sun, S.-H. (2003). Reduction of flow-induced forces on a circular
780 cylinder using a detached splitter plate. Physics of Fluids, 15, 2433–2436.

781 Jain, A., Jones, N.P., & Scanlan, R.H. (1996). Coupled flutter and buffeting analysis of long-
782 span bridges. Journal of Structural Engineering, 122, 716–725.

783 Jebelli, M., & Masdari, M. (2022). Interaction of free oscillating flat plate and VIV of a circular
784 cylinder in laminar flow. Journal of Fluids and Structures, 113, 103648.
785 https://doi.org/10.1016/j.jfluidstructs.2022.103648

786 Lin, S.-Y., & Wu, T.-M. (1994). Flow control simulations around a circular cylinder by a finite
787 volume scheme. Numerical Heat Transfer Part A: Applications, 26, 301–319.

788 Mittal, C., & Sharma, A. (2022). Flow-induced coupled vibrations of an elastically mounted
789 cylinder and a detached flexible plate. Journal of Fluid Mechanics, 942, A57.

790 Parkinson, G. (1989). Phenomena and modelling of flow-induced vibrations of bluff bodies.
791 Progress in Aerospace Sciences, 26, 169–224.